Measuring Bedload Sediment Transport with an Acoustic Doppler Velocity Profiler

Koen Blanckaert, Joris Heyman, Colin D Rennie

To cite this version:

Koen Blanckaert, Joris Heyman, Colin D Rennie. Measuring Bedload Sediment Transport with an Acoustic Doppler Velocity Profiler. Journal of Hydraulic Engineering, 2017, 143 (6), pp.04017008. ⟨10.1061/(ASCE)HY.1943-7900.0001293⟩. ⟨hal-01518505⟩

HAL Id: hal-01518505

https://univ-rennes.hal.science/hal-01518505v1

Submitted on 8 Dec 2020

Measurements of bedload sediment transport with an Acoustic Doppler Velocity Profiler (ADVP)

Koen Blanckaert[1], Joris Heyman[2], Colin D. Rennie[3]

[1] Ecological Engineering Laboratory, ENAC, Ecole Polytechnique Fédérale Lausanne, Switzerland. koen.blanckaert@epfl.ch

Distinguished visiting researcher, University of Ottawa

[2] UMR CNRS 6251, Institut de Physique de Rennes, 35042, Rennes, France (joris.heyman@univ-rennes1.fr)

[3] University of Ottawa, Ottawa, ON, K1N 6N5, Canada.Email: Colin.Rennie@uottawa.ca

ABSTRACT (250 words)

Acoustic Doppler Velocity Profilers (ADVP) measure the velocity simultaneously in a linear array of bins. They have been successfully used in the past to measure three-dimensional turbulent flow and the dynamics of suspended sediment. The capability of ADVP systems to measure bedload sediment flux remains uncertain. The main outstanding question relates to the physical meaning of the velocity measured in the region where bedload sediment transport occurs. The main hypothesis of the paper, that the ADVP measures the velocity of the moving bedload particles, is validated in laboratory experiments that range from weak to intense bedload transport. First, a detailed analysis of the raw return signals recorded by the ADVP reveals a clear footprint of the bedload sediment particles, demonstrating that these are the main scattering sources. Second, time-averaged and temporal fluctuations of bedload transport derived from high-speed videography are in good agreement with ADVP estimates. Third, ADVP based estimates of bedload velocity and thickness of the bedload layer comply with semi-theoretical expressions based on previous results. An ADVP configuration optimized for bedload measurements is found to perform only marginally better than the standard configuration for flow measurements, indicating that the standard ADVP configuration can be used for sediment flux investigations. Data treatment procedures are developed that identify the immobile-bed surface, the layers of rolling/sliding and saltating bedload particles, and the thickness of the bedload layer. Combining ADVP measurements of the bedload velocity with measurements of particle concentration provided by existing technology would provide the sediment flux.

KEY WORDS

bedload transport, acoustics, three-dimensional acoustic Doppler velocity profiler (3D-ADVP), digital videography, particle velocimetry, optical flow

HIGHLIGHTS

1. Signature of signal, simultaneous video analysis and agreement with semi-theoretical formulae demonstrate that ADVP can measure bedload velocities and bedload layer thickness.
2. ADVP measures time-averaged and turbulent velocities of bed load particles.
3. ADVP analysis identifies immobile-bed surface, and layers of rolling/sliding and saltating bedload.

INTRODUCTION

Problem definition

Knowledge of the quantity of sediment transported in rivers is of paramount importance, for example for understanding and predicting morphological evolution, hazard mapping and mitigation, or the design of hydraulic structures like bridge piers or bank protections. In spite of this importance, measurement of the sediment flux is notoriously difficult, especially during high flow conditions when most sediment transport occurs.

The sediment flux per unit width can be expressed as:

$$q_s = \int_{z_b}^{z_s} u_s c_s dz \tag{1}$$

where z_s is the water surface level, z_b the immobile bed level, u_s the sediment velocity, and c_s the sediment concentration. The total sediment flux is the most relevant variable with respect to the river morphology. It is, however, often separated in fluxes of suspended load sediment transport and bedload sediment transport. Suspended load refers to sediment particles that are transported in the body of the flow, being suspended by turbulent eddies. Because of their small size – and thus their small Stokes number – suspended particles tend to follow the flow streamlines, and thus their velocities are close to the velocities of the turbulent flow. In contrast, bedload involves larger sediment particles that slide, roll and saltate on the bed, thus remaining in close contact with it. The friction and the frequent collisions of bedload particles with the granular bed reduce considerable their velocity. Because of drag forces, fluid velocities may also be reduced inside the bedload layer.

Accurate measurement of bedload transport has long been a goal of river and coastal scientists and engineers (e.g., Mulhoffer 1933). Conventional measurements with physical samplers are limited in spatial and temporal resolution, are cost prohibitive due to substantial manual labour, and can be difficult and/or dangerous to conduct during high channel-forming flows when most bed material transport occurs. Videography techniques have been developed for laboratory settings and well-controlled flows (Drake et al. 1988, Radice et al. 2006, Roseberry et al. 2012, Heyman 2014), but are hindered when intense suspended sediment transport occurs due to the turbidity of the water. They are particularly difficult to use in the field especially under high flow conditions when intense sediment transport occurs. Consequently, little is known about the temporal and particularly the spatial distribution of fluvial bedload, other than the recognition that the spatiotemporal distribution of bed material transport determines channel form (Ferguson et al. 1992, Church 2006, Seizilles et al. 2014; Williams et al. 2015).

Acoustic Doppler Current Profiler (ADCP) backscatter intensity and/or attenuation have been used to estimate suspended sediment concentration and grain size (e.g., Guerrero et al. 2011; Guerrero et al. 2013; Moore et al. 2013; Latosinski et al. 2014; Guerrero et al. 2016). Rennie et al. (2002), Rennie and Church (2010), and Williams et al. (2015) have used the bias in ADCP bottom tracking (Doppler sonar) as a measure of apparent bedload velocity. Due to the diverging beams of ADCP's, this technique may provide only an indication of bedload particle velocities averaged over the bed surface insonified by the four beams. This technique also does not provide the thickness and concentration of the active bedload layer, which are required to determine the bed load flux (Rennie and Villard 2004; Gaueman and Jacobson 2006).

ADVP's, which use beams that converge in one single area of measuring bins, have commonly been used to investigate turbulent flows (Figure 1). Their application range has recently been extended to the investigation of the dynamics of transported sediment, mainly transport in suspension (e.g., Crawford and Hay 1993; Thorne and Hardcastle 1997; Shen and Lemmin 1999; Cellino and Graf 2000; Stanton 2001; Smyth et al. 2002; Thorne and Hanes

2002, Hurther et al. 2011; Thorne et al. 2011; Thorne and Hurther 2014). The present paper focuses on their use for the measurement of bedload sediment transport.

ADVP: working principle and state-of-the-art

The working principle of ADVP has been detailed previously (e.g., Lemmin and Rolland 1997 ; Hurther and Lemmin 1998; Thorne et al. 1998; Shen and Lemmin 1999; Stanton and Thornton 1999; Stanton 2001; Zedel and Hay 2002). The main features of the ADVP's working principle that are required for making the present paper self-contained are summarized hereafter. An ADVP consists of a central beam emit transducer surrounded by multiple fan-beam receive transducers (Figure 1a). The instrument is typically set up on a fixed mount pointing down toward the bed, and measures simultaneously velocities in the water column situated between the emitter and the bed. This water column is divided in individual bins of O(mm). The profiling range, i.e. the height of the measured water column, is typically of O(m). The emit transducer sends a series of short acoustic pulses vertically down towards the bed with a user-defined pulse-repetition-frequency (PRF) and pulse length. These pulses are reflected by scattering sources in the water, and a portion of this scattered sound energy is directed toward the receive transducers. Turbulence-induced air bubble microstructures in sediment-free clear water (Hurther, 2001) or sediment particles in sediment-laden flows (Hurther et al. 2011) can be scattering sources of this instrument. For each bin in the water column, the backscattered signal recorded by each of the receivers can be written as:

$$a(t) = A\cos[2\pi(f_0 + f_D)t] \qquad (2)$$

A is the amplitude of the recorded signal and f_D the Doppler frequency shift. The latter is proportional to the velocity component directed along the bisector of the backscatter angle (Figure 1b):

$$f_D = 2\frac{f_0}{c}\vec{V}.\vec{e}_B \qquad (3)$$

The speed of sound in water is indicated by c, $\vec{V}$ is the vectorial velocity of the scattering source, $\vec{e}_B$ the unit vector along the bisector of the backscatter angle for the considered bin. In order to compute f_D, the recorded signal $a(t)$ is typically demodulated into in-phase and quadrature components, represented by $I(t)$ and $Q(t)$, measured in volt. The Doppler frequency $f_D(t)$ corresponds to the frequency of these oscillating $I(t)$ and $Q(t)$ signals. The demodulation into in-phase and quadrature parts is necessary to determine the sign of f_D. The quasi-instantaneous Doppler frequency is typically computed with the pulse-pair algorithm using NPP (number of pulse-pairs) samples of $I(t)$ and $Q(t)$ (Miller and Rochwarger 1972; Lhermitte and Serafin, 1984; Zedel et al. 1996; Zedel and Hay 2002):

$$\hat{f}_D = \frac{PRF}{2\pi}\tan^{-1}\left[\frac{\sum_{s=1}^{NPP-1} Q_s I_{s+1} + I_s Q_{s+1}}{\sum_{s=1}^{NPP-1} I_s I_{s+1} + Q_s Q_{s+1}}\right] \qquad (4)$$

The symbol ^ denotes an average over NPP time samples, and s denotes a time index. NPP has to be chosen high enough to assure second-order stationarity, but low enough so that NPP/PRF remains small compared to the characteristic timescale of the investigated turbulent flow. Utilization of at least three receive transducers allows for measurement of all three velocity components. Beam velocities are converted to Cartesian coordinates using a beam transformation matrix specific for the beam geometry.

[Figure 1]

Acoustic Concentration and Velocity Profilers (ADCP), which integrate an ADVP and an Acoustic Backscatter System (ABS), have been successfully used to investigate suspended sediment fluxes, defined as the product of sediment velocity and sediment concentration

(Equation 1). The ADVP measures the velocity of the suspended sediment, which is assumed to be equal to the flow velocity. The ABS provides the particle concentration in bins throughout a profile is obtained based on the range-gated acoustic backscatter intensity and/or attenuation (e.g., Crawford and Hay 1993; Thorne and Hardcastle 1997; Shen and Lemmin 1999; Thorne and Hanes 2002; Hurther et al. 2011; Thorne et al. 2011; Thorne and Hurther 2014; Wilson and Hay 2015; Wilson and Hay 2016). These measurements have permitted direct examination of suspended sediment transport as a function of flow forcing. For example, Smyth et al. (2002) used an ADCP system to document periodic sediment suspension associated with turbulent vortex shedding from ripples in a wave bottom boundary layer.

A broadband multifrequency ADCP, called MFDop, capable of 0.0009 m vertical resolution at 85 Hz has recently been developed by Hay et al. (2012a,b,c), that allows for estimation of both particle concentration and grain size (Crawford and Hay 1993; Thorne and Hardcastle 1997; Wilson and Hay 2015; Wilson and Hay 2016). For this system, velocities measured in bins within 0.005 m of a fixed bed were deemed to be negatively biased, based on nonconformity with the profiles of both log-law velocity and phase shift expected in a wave bottom boundary layer. This bias occurred largely because equal travel time paths between send and receive transducers included bottom echo for bins close to the bed (Figure 1a,b). However, the system was able to measure the bed velocity (of an oscillatory cart) based on Doppler processing of the signal at the observed bottom range.

Hurther et al. (2011) have recently developed ACVP, which combines an ADVP with advanced noise reduction for turbulence statistics (Blanckaert and Lemmin 2006, Hurther and Lemmin 2008) with the ABS system developed by Thorne and Hanes (2002). The ACVP measures co-located, simultaneous profiles of both two-component velocity and sediment concentration referenced to the exact position at the bed. Measurements are performed with high temporal (25 Hz) and spatial (bin size of 0.003 m) resolution. Sediment concentration profiles are determined by applying the dual-frequency inversion method (Bricault 2006; Hurther et al. 2011), which offers the unique advantage of being unaffected by the non-linear sediment attenuation across highly concentrated flow regions, and thus to allow also for the measurement of high sediment concentrations near the bed where the bedload transport occurs. The acoustic theory underpinning the dual-frequency inversion method is based on the condition of negligible multiple scattering (Hurther et al. 2011). Although this condition is probably violated in the bedload layer, Naqshband et al. (2014b, their Figure 12) have successfully applied the method to estimate the sediment concentration all through the bedload layer onto the immobile bed, where a bulk concentration of $\rho_s(1-\varepsilon)$ = 1590 kg m^{-3} was correctly measures. Here ε is the porosity of the immobile sediment bed. These results indicate that the theoretical condition of negligible multiple scattering can be relaxed and that the dual-frequency inversion method is also able to measure the high sediment concentrations in the bedload layer. The ACVP has been used to measure velocity, concentration profiles and sediment fluxes over ripples under shoaling waves (Hurther and Thorne 2011) and over migrating equilibrium sand dunes (Naqshband et al. 2014a,b). An acoustic interface detection method was used to identify the immobile bed and the suspended load layer and a layer in between with higher sediment concentrations (Hurther and Thorne 2011; Hurther et al. 2011). Hurther and Thorne (2011) acknowledged uncertainty in the identification of the near-bed layer with high sediment concentration, but found that the estimated sediment flux matched estimates based on ripple migration. They termed this layer the “near-bed load layer”. Naqshband et al. (2014b) also found that sediment fluxes in this layer were in line with estimates for bedload transport. Measured velocities in this layer were found to deviate from the logarithmic profile often observed above plane immobile beds. These deviations were attributed to the presence of the high sediment concentration. There remains uncertainty, however, in the physical meaning of the velocities measured in this non-logarithmic velocity layer. This uncertainty is acknowledged by Naqshband et al. (2014b), who note that it is difficult to validate whether this layer corresponds to the physical bedload layer, because no data could be collected to trace sediment movement or sediment paths.

These recent developments clearly demonstrate that ADCP systems are capable of measuring suspended load sediment flux, but that the capability of ADCP systems to measure bedload sediment flux remains uncertain. The ABS component of the system's ability to measure sediment concentration in the bedload layer has been demonstrated (Naqshband et al. 2014b). The main outstanding question relates to the physical meaning of the velocity measured by the ADVP component of the system in the region where bedload sediment transport occurs (Equation 1).

Other issues remain that render uncertain the capability of ADVP systems to measure bedload. First, 3D acoustic velocity profilers are usually configured to obtain optimal measurements of flow properties. Typically, an ADVP is set up such that the region of overlap of the emit and receive beams maximizes the profiling range and includes the entire water column, such that optimal measurements of flow properties are obtained in the core of the water column (Figure 1a). This means that the axis of the receiver, where the receivers' sensitivity is highest, intersects the insonified water column in a bin displaced above the bed in the body of the water column. Moreover, the acoustic power is optimized in the water column, in order to maximize the signal-to-noise ratio (SNR). This commonly leads to a power level of the backscatter for bins near the bed that is outside the recording range of the receivers, because the acoustic backscatter from bedload sediment particles is much greater than from scattterers in the water (Figure 2). Second, there is potential for contamination of near-bed bins by high intensity scatter from the immobile bed with equivalent acoustic travel time between the send and receive transducers (Figure 1a,b). As discussed above, this can result in negative bias of particle velocities estimated in near-bed bins (Hay et al. 2012a). This can also result in saturation of the first bin echo, which makes difficult the estimation of Doppler velocity and particle concentration. Similarly, highly concentrated bedload in the first bin can saturate the echo from the first bin. Third the nature of bedload itself renders the scattering and propagation within the bedload layer complex. The usual scattering model assumes a low concentration of scatterers in the water. This assumption is most probably violated in the bedload layer. Moreover, bedload particle sizes and velocities are variable, thus bedload transport tends to be a heterogeneous phenomenon, which broadens the received frequency spectrum and could render Doppler velocity estimates imprecise. Bed material particle size distributions tend to be log-normal, and bedload particle velocity distributions can be left skewed gamma (Drake et al. 1988, Rennie and Millar 2007), exponential (Lajeunesse et al. 2010; Furbish et al. 2012) or Gaussian (Martin et al. 2012, Ancey and Heyman 2014). Conventional Doppler signal processing techniques find the mean velocity in a presumed homogenous volume of particles, and this estimate may not best characterize the bedload.

[Figure 2]

Hypothesis and detailed objectives

The main objective of the present paper is to demonstrate the capability of ADVP systems to measure bedload sediment transport, by investigating the physical meaning of the velocity measured with the ADVP in the region where bedload sediment transport occurs. In all experiments without sediment transport reported in this paper, the ADVP resolved the law of the wall logarithmic velocity profile, including very close to the bed (Figure 3a). On the contrary, in all experiments with bedload sediment transport reported in this paper, velocities in the near-bed region where bedload sediment transport occurs were found to deviate from the logarithmic profile (Figure 3a,b), similar to observations Naqshband et al. (2014b). The main hypothesis of the present paper is that the ADVP measures the velocity of the sediment particles moving as bedload in this near-bed region. The hypothesis is tested over a range of bedload transport conditions for a gravel-sand bed material mixture in a mobile bed flume. In this paper we focus on measurement of bedload particle velocities and the thickness of the bed load layer. In order to validate the hypothesis, three strategies are followed. First, a detailed analysis is performed of the raw $I(t)$ and $Q(t)$ signals recorded by the ADVP's receivers that reveals a clear footprint of the bedload sediment particles. Second, simultaneous observations of bedload sediment transport are conducted with high speed digital videography. Third, ADVP based estimates of the bedload velocities and thickness of the bedload layer are compared to semi-theoretical formulae based on previous results.

The present research makes use of an ADVP configuration that is specifically designed and tested for measurement of bedload transport. As described below, the instrument beam geometry is designed such that it is most sensitive in the first bin above the bed, and the acoustic power is chosen such that backscattered signal remains within the recording range of the receivers in the bedload region (Figure 2). The bedload measurement capabilities of this optimised ADVP configuration and the standard ADVP configuration for flow measurements are also compared.

[Figure 3]

METHODS

Experimental program

The ADVP's potential to measure bedload was tested in a flume at École Polytechnique Fédéral de Lausanne (EPFL). The flume was 0.50 m wide with zero slope, and the test section was 6.6 m downstream of the flume inlet. The bed sediment was poorly sorted ($\sigma = 0.5 \times (d_{84}/d_{50} + d_{50}/d_{16}) = 4.15$, where d_i represents the ith percentile grain size) with median, mean, and 90th percentile grain sizes of d_{50}=0.0008 m, d_m = 0.0023 m and d_{90} = 0.0057 m, respectively (Leite Ribiero et al. 2012). The critical shear velocity for the initiation of sediment transport for d_{50} and d_m are 0.020 m s^{-}1 and 0.039 m s^{-1}, respectively, based on the Shields criterion (Shields 1936). No sediment was fed to the flume or recirculated during the tests. The transported sediment originated from the entrance reach of the flume, where erosion locally occurred. Between experiments, the scour hole was replenished to compensate for sediment lost from the system. Due to the inherent intermittency and variability of sediment transport (Drake et al. 1988, Frey et al. 2003, Singh et al 2009; Heyman et al. 2013; Mettra 2014) and the formation of small dunes, bed levels varied during some of the tests. These conditions were chosen on purpose, in order to provide a broad range of experimental conditions, and to test the robustness of ADVP bedload measurement in quasi-realistic conditions. Table 1 summarizes the conditions in all experiments.

The main series of tests utilized simultaneously both the ADVP in a configuration optimized for the measurement of bedload transport (Figure 1b), and a digital video camera for bedload measurement (Figure 1c). The nominal flow depth was 0.24 m, but varied slightly between test runs (Table 1). This flow depth was obtained by regulating a weir at the downstream end of the flume. Three bedload transport conditions were tested by changing the flow rate in the flume. The low flow run Q630 (Q = 0.063 m^3 s^{-1}) resulted in dune transport of fine sediment (smaller than d_m) that led to gradual armouring of the bed. The medium flow run Q795 (Q = 0.080 m^3 s^{-1}) produced partial transport conditions, with coarser particles in transport, but many of the coarse particles on the bed surface were stable at any particular instant. Lastly, the high flow run Q1000 (Q = 0.100 m^3 s^{-1}) broke up the armour bed and the entire bed surface and all grain sizes were mobile throughout the run. At these highest flow conditions, the saltation height and length of bedload particles were considerably increased, but suspended load sediment transport remained negligible. The Shields parameters based on

d_{50} and d_m varied from 0.07 to 0.24 and from 0.02 to 0.08, respectively, in these experiments. The sediment transport behaviour was in agreement with expectations based on the Shields parameter and the critical shear velocity for the different grain sizes in the sediment mixture (Bose and Dey 2013). Videos of the three sediment transport conditions are available as supporting information. Measurements with high and low acoustic power were utilized and compared for each bedload transport condition (Figure 2). The high acoustic power corresponds to the standard ADVP setting, where SNR is optimized in the main body of the water column, but leads to frequent saturation of the signal in the near-bed area. The low acoustic power minimizes potential for acoustic saturation of the near-bed layer. It is expected to improve measurements in the near-bed layer, but leads to a lower SNR in the main body of the water column. The labels of experiments with high and low acoustic power are appended with H and L, respectively (Table 1).

[Table 1]

A second series of tests was also collected with the ADVP in its standard configuration optimized for flow measurements in the body of the water column (Figure 1a), and without simultaneous videography (Table 1). The purpose of this series was to compare the capabilities of the standard ADVP configuration and the one optimized for bedload measurements, and to extend the investigation to a broader range of hydraulic conditions. Experiments were performed with nominal flow depths of 0.14 m and 0.24 m. For each of these flow depths, 10 different discharges were tested (Table 1). In the tests with 0.14 m flow depth, discharge ranged from 0.013 $m^3 s^{-1}$ to 0.060 $m^3 s^{-1}$, shear velocity from 0.009 $m s^{-1}$ to 0.052 $m s^{-1}$ and the Shields parameters based on d_{50} and d_m from 0.006 to 0.20 and from 0.002 to 0.07, respectively. In the tests with 0.24 m flow depth, discharge ranged from 0.020 $m^3 s^{-1}$ to 0.100 $m^3 s^{-1}$, shear velocity from 0.012 $m s^{-1}$ to 0.062 $m s^{-1}$ and the Shields parameter based on d_{50} and d_m from 0.01 to 0.29 and from 0.003 to 0.10, respectively. At the lowest discharge, no sediment transport occurred, whereas generalized and intense sediment transport occurred at the highest discharge. Again, the sediment transport behaviour was as expected based on the Shields parameter and the critical shear velocity for the different grain sizes in the bed mixture (Bose and Dey 2013). The runs with 0.24 m flow depth encompassed the hydraulic conditions investigated in the main series with optimized ADVP configuration and simultaneous videography, which facilitates comparison.

ADVP configuration and data analysis procedures

The ADVP utilized for this research has been developed at EPFL. Its working principle has been detailed in Rolland and Lemmin (1997), Hurther and Lemmin (1998, 2001), Hurther (2001), and Blanckaert and Lemmin (2006). The instrument consists of a central emit transducer of diameter 0.034 m and of carrier frequency, f_0 = 1 MHz, with beam width of 1.7°, and four 30° fan-beam receive transducers that are 30° inclined from the vertical (Figure 1). In all experiments, PRF was set to 1000 Hz, and NPP to 32, yielding a sampling frequency of PRF/NPP = 31.25 Hz for the quasi-instantaneous Doppler frequencies and velocities. A pulse length of 5 μs was chosen, yielding a vertical resolution of velocity bins of about 0.004 m. A time series of more than 10 min was collected for each test condition, which was sufficient to obtain statistically stable measurements of the flow and sediment transport under quasi-steady conditions. Blanckaert and de Vriend (2004) and Blanckaert (2010) discuss in detail the uncertainty in the flow quantities measured with this ADVP. They report a conservative estimate of 4% uncertainty in the streamwise velocity u.

In the main series of tests (Table 1), the ADVP configuration was optimized to measure bedload transport, as explained hereafter (Figure 1b). The ADVP was configured symmetrically, with horizontal and vertical distances between emit and receive transducers of 0.1305 m and 0.0304 m, respectively. The ADVP was immersed in the flow, with the emit transducer 0.185 m above the nominal bed level. With this configuration, the centre of the receive beam was focused on the bed level. This ensured that the ADVP was most sensitive in the vicinity of the bedload layer. This configuration, however, did not allow for measurements in the upper half of the water column (Figure 1b).

In the second series of experiments (Table 1), the standard ADVP configuration was used (Figure 1a). Receivers symmetrically surrounded the emit transducer at horizontal and vertical distances of 0.1343 m and 0.0295 m, respectively. In order to measure the entire water column, the ADVP was placed about 7 cm above the water surface in a water-filled box that was separated from the flowing water with an acoustically transparent mylar film (Figure 1a). The box induces perturbations of the flow in a layer with a thickness of about 0.02m near the water surface. In the experiments with flow depth of 0.14 m, the center of the receive beam was focused on the bed level. In the experiments with flow depth of 0.24 m, it was focused in the core of the water column, about 0.10 m above the bed (Figure 1a).

The acoustic footprint on the bed of the emitted beam is circular with a diameter that ranges from about 0.045 m in the experiments with 0.14 m flow depth to about 0.055 m in the experiments with 0.24 m flow depth (Figure 1). This means that the ADVP does not resolve grain scale processes, but processes at a characteristic scale of about 0.05 m.

The standard ADVP data analysis procedure considers two output quantities: the magnitude of the backscattered signal recorded by the receive transducers (Figure 2) and the time-averaged velocity estimated with the pulse-pair algorithm (Equation 4, Figure 3).

The profile of the time-averaged longitudinal flow velocity is typically logarithmic in the vicinity of the bed in cases without bedload sediment transport (Nezu and Nakagawa, 1993). In order to identify the logarithmic part, the measured time-averaged velocity is plotted as a function of $\log(30z/k_s)$, where z is the distance in meter above the immobile bed, and the equivalent grain roughness k_s is taken as 0.01 m (Figure 3). In order to avoid singularities, the bin containing the surface of the immobile bed has been plotted at $z = 0.001$ m. The profile of the time-averaged velocity as a function of $\log(30z/k_s)$ also identifies the near-bed region where the measured velocities are smaller than the logarithmic profile in cases with bedload sediment transport, similar to observations by Naqshband et al. (2014b). In this non-logarithmic near-bed layer, the measured velocity profiles typically have an S-shape (Figure 3). As mentioned before, the main hypothesis of the present paper is that the ADVP measures the particle velocities in this near-bed zone. Sediment is predominantly moving as bed load transport in the investigated experiments. Most particles are intermittently entrained from the immobile bed by the flow, slide and roll over the immobile bed, and finally immobilize again. The velocity of these sliding and rolling particles is generally smaller than the velocity of the surrounding fluid, due to momentum extraction by inter-particle collisions, inertia of the sediment particles, and friction on the granular bed. The difference between the velocities of particles and the entraining flow is called the slip velocity (Nino and Garcia 1996; Muste et al. 2009). It is assumed that the extrapolated logarithmic profile provides an estimate of the velocity of the entraining flow. An increase in number of moving particles can be assumed to increase the momentum extraction due to inter-particle collision, and hence also the slip velocity. Therefore, the dominant bed load transport is assumed to occur at the elevation of maximum slip velocity, which approximately coincides with the inflection point in the S-shaped near-bed velocity profile (Figure 3b). By definition, this inflection point occurs where the second derivative of the velocity with respect to z vanishes. Some bedload particles saltate on the bed and reach higher elevations in the water column. Because saltating bedload particles are usually relatively small and their saltation length scale is longer with fewer inter-particle collisions than those of the rolling bedload particles, their velocity is closer to the velocity of the entraining fluid. As mentioned before, suspended load particles have negligible slip velocity and move at about the same velocity as the flow. Thus, the shape of the measured velocity profile identifies the layer with rolling and sliding bedload transport, the layer with saltating bedload transport and the layer with suspended load transport or clear water.

A critical issue in the identification of the different layers of sediment transport is the identification of the elevation of the surface of the immobile bed, which by definition corresponds to zero velocity. The accuracy in the identification of the immobile bed surface is limited by the finite bin size of 0.004 m and by the fact that a natural sediment bed is not perfectly planar. The best practice consists in identifying the bin in which the surface of the immobile bed is situated, as illustrated in Figure 4. The upper part of that bin will be situated in the flow. In case no bedload sediment transport occurs, the ADVP will measure zero velocity in the bin containing the surface of the immobile bed, because the magnitude of the raw signal backscattered on micro-air bubbles in the flowing water is much smaller than the magnitude of the one backscattered on the immobile bed. If bedload sediment particles roll and slide on the immobile bed within the bin containing the immobile bed, the ADVP will measure a non-zero velocity, which corresponds to the average velocity of sediment particles within that bin (Figure 4), i.e. this spatial average also includes areas of zero velocity associated with immobile particles within the measuring area of the ADVP. The bin containing the surface of the immobile bed is therefore identified as the bin with the minimum non-zero velocity, as illustrated in Figures 3 and 4.

A second independent estimation of the bin containing the surface of the immobile bed is obtained from the magnitude of the raw backscattered signal recorded by the receivers, $I^2 = 0.25\ (I_1^2+I_2^2+I_3^2+I_4^2)$ (Figure 2). Here, I_1, I_2, I_3 and I_4 are the raw in-phase components of the demodulated signals recorded by each of the four receivers. The magnitude of the backscattered signal relates to the concentration of the sediment particles, because sediment particles backscatter considerably more acoustic energy than micro air-bubbles in the water column above (Hurther et al. 2011). Based on this heuristic definition, the bin containing the immobile bed is assumed to correspond to the peak in the profile of the magnitude of the backscattered signal (Figure 2). In the present paper, we have used the first estimation to define the bin containing the surface of the immobile bed, and the second estimation for validation purposes. In general, both estimation identified the same bin.

In the Q795L experiment shown in Figures 2 and 3b, the surface of the immobile-bed is estimated within bin number 58, the sliding and rolling bedload is estimated in bin 57, and the top of the saltating bedload in bin 55. These heuristic estimations are based on the shape of the velocity profile as discussed earlier. In most experiments, however, the bed load sediment transport caused variations in the elevation of the surface of the immobile bed during the 10 min duration of the experiment. This is illustrated for experiment Q1000L in Figure 5, which shows the temporal evolution of the magnitude of the raw backscattered return signal, $I^2 = 0.25\ (I_1^2+I_2^2+I_3^2+I_4^2)$, during the 614 s measurement period. The figure highlights the part of the water column between bin numbers 50 and 65 where the magnitude of the backscattered raw return signal reaches maximum values. This range encompasses the immobile bed, the assumed layers of rolling/sliding and saltating bedload, and part of the clear water layer. Variations in the elevation of the surface of the immobile bed level are clearly illustrated by the temporal evolution of the location where the maximum magnitude of the raw return signal occurs. The bed level aggraded in the beginning of the test and reached a maximum level after approximately 60 s. The bed level subsequently gradually lowered and reached a quasi-constant level after approximately 165 s. Periods with quasi-constant characteristics are first identified and isolated in each experiment (see Table 2 and detailed Tables in the supporting information). For the Q1000L experiment shown in Figure 5, for example, 5 periods of quasi-constant conditions are identified. The data analysis procedure of the ADVP measurements is performed separately for each of these periods. For each period of quasi-constant conditions the elevation of the surface of the immobile bed, the layer of saltating bedload, the layer of rolling and sliding bedload, and the layer of sediment-free clear water are defined based the data analysis procedures described above. These layers are indicated in all relevant figures.

[Figure 5]

Digital videography

A Basler A311f high-speed digital video camera was used to record images of the mobile bed through the sidewall of the flume (Figure 1c). The images gave a distorted picture of the bed (due to perspective) but were centred on the ADVP sample volume in the centre of the flume, with a 0.122 m centreline longitudinal by 0.155 m transverse field of view. The images had 656x300 resolution, thus pixel size was approximately 0.0002x0.0005 m. The videography maps the three-dimensional sediment motion on a horizontal plane, which is complementary to the resolution in a vertical water column provided by the ADVP. Image exposure time was 300 μs, and sampling rate was 111 Hz. Computer clock times were used to synchronize image acquisition with ADVP data collection. Digital video images were orthorectified using a projective transformation (Beutelspacher et al. 1999). Due to limitations in computer storage and data transfer, digital videos with high temporal resolution could only be recorded for maximum 10 seconds. During the 10-minute ADVP data collection, 10-second digital videos were collected once every minute (Figure 5). The cumulative duration of the digital videos of more than 110 seconds is long enough to obtain reliable estimates of the velocities of the bedload particles. Two complementary image treatment algorithms were used.

In order to estimate the velocity of sediment particles, the robust open-source particle tracking velocimetry (PTV) algorithm *PolyParticleTracker* was used (Rogers et al. 2007). This algorithm is able to estimate the position and track several objects through frames with a sub-pixel resolution. The algorithm was specifically developed for tracking bright objects over a complex background. The particle instantaneous velocities are then estimated by time differentiation of the particle positions. Erroneous trajectories were filtered with techniques commonly used in Particle Image Velocimetry. First, a maximum acceleration criterion of 40 m s^{-2} was defined for individual particles. Then, the angle between two successive velocity vectors was limited to 90°. Particles are often found with velocities close to zero while bouncing on the bed. In order to avoid sampling of these quasi-immobile bed particles that only marginally contribute to the sediment flux, a minimum velocity threshold of 0.04 m s^{-1} was adopted. Full trajectories of particles, from entrainment to deposition were not always recovered by the algorithm, mainly due to the presence of the noisy background composed of resting particles. Moreover, not all of the moving particles were systematically detected. It can be expected that especially the saltating bedload with relatively small grain size and relatively high velocities was undersampled. Enough particle trajectories were correctly recovered to provide a good estimate of the distribution functions of the sediment velocities and the time-averaged velocity of the moving sediment particles. These quantities will be shown and discussed in the section “Simultaneous videography”.

An instantaneous spatio-temporal quantification of the bedload layer velocities was, however, not possible from the trajectories obtained with the PTV method, since not all of the moving particles were systematically detected by the automated algorithm and since full trajectories from entrainment to deposition were not always recovered. In order to estimate bedload velocity time series in the ADVP sample volume, a complementary analysis of the digital video images was performed with the Optical Flow algorithm (Horn and Schunck 1981). This algorithm remediates the small sample limitation of the particle tracking algorithm by computing for each pair of frames a dense 2D velocity field that reflects the local apparent motion in the image. The algorithm assumes that the intensity value $I(x,y,t)$ of each pixel follows a simple advection equation :

$$\frac{\partial I}{\partial t}+u\frac{\partial I}{\partial x}+v\frac{\partial I}{\partial y}=\varepsilon \qquad (5)$$

where the problem unknowns are the velocity components $u(x,y,t)$ and $v(x,y,t)$ along the x and y axes. The partial derivatives of I can be estimated directly from the video stream: $\partial I/\partial t$ is the temporal change in pixel intensity, and $\partial I/\partial x$ and $\partial I/\partial y$ are the spatial gradients in pixel intensity. The Optical Flow method determines the velocity field (u,v) that minimize ε. Intuitively, the apparent motion of an object is better appreciated by the human eye if it contains high intensity gradients (border contrasts for instance). On the contrary, the motion of objects with low contrast is difficult to estimate by the human eye. This is similar for the Optical Flow method, which will perform better when $\partial I/\partial x$ and $\partial I/\partial y$ are larger. In case these spatial gradients equal zero, the velocity field (u,v) is not uniquely determined by Equation (5) and the problem is ill-posed. In this case, an additional constraint (also called a regularizer Horn and Schunck 1981) needs to be imposed, usually based on the continuity of the velocity field. The efficiency of this technique relies thus on the presence of strong intensity gradients, as those frequently observed at object edge contours. The Optical Flow algorithm can be expected to be especially appropriate for the largest bedload particles that roll and slide on the immobile bed, because these particles form well distinguishable contours in the digital images that yield large gradients $\partial I/\partial x$ and $\partial I/\partial y$. Faster and smaller bedload particles can be expected to be undersampled due to their weaker intensity gradients. This algorithm has been successfully applied in numerous applications, including flow reconstruction from Particle Image Velocimetry techniques (Ruhnau et al. 2005, Heitz et al. 2008), but it has yet rarely been applied to the estimation of sediment motion (Spies et al. 1999, Klar et al. 2004). Here, the Optical Flow algorithm has been applied to investigate the time-resolved velocity of the bedload particles inside the ADVP sample volume. The particle velocities have been estimated from the digital video images with the open access Matlab implementation of the Lukas-Kanade Method (Lucas and Kanade, 1981) by Stefan M. Karlsson and Josef Bigun and available at http://www.mathworks.com/matlabcentral/fileexchange/40968. In order to improve the accuracy and to reduce noise, the velocity field was averaged on a 70x70 grid overlapping the original 656x300 pixels images. The local sediment velocity spatially-averaged within the footprint of the ADVP's measuring beam at the bed was then obtained by averaging the 70x70 Optical Flow velocity field using a Gaussian kernel centred on the volume. It is worth noting that this spatial average also includes areas of zero velocity associated with immobile particles, and thus reflects the average bed velocity. This is different from the sediment velocities estimated with the PTV algorithm, which only considers moving sediment particles. It is similar, however, to the velocities measured by the ADVP in the bin containing the surface of the immobile bed (cf. section "ADVP configuration and data analysis procedures"). The temporal fluctuations of this locally spatially averaged velocity will be shown and discussed in the section "Simultaneous videography".

RESULTS

Signature of the raw signals recorded by the ADVP

Most commercial ADVP systems only provide as output the quasi-instantaneous Doppler frequencies or velocities sampled at PRF/NPP. The ADVP used in the present investigation also provides the backscattered raw return signals recorded by the receivers, *I* and *Q*, sampled at PRF. This is a major advantage, as it allows analysing the raw signals for the presence of a footprint of bedload sediment transport. This analysis will be illustrated for the Q795L experiment, where the bed level remained stable during the entire 624 s of continuous measurements.

First, the time-averaged magnitude of the backscattered raw return signal, $I^2 = 0.25 (I_1^2+I_2^2+I_3^2+I_4^2)$ is considered (Figure 2). The magnitude of the backscattered signal relates to the concentration of the sediment particles, because sediment particles backscatter considerably more acoustic energy than micro air-bubbles in the water column above (Hurther et al. 2011). The magnitude of the return signal decreases with distance upwards from the immobile bed level, which complies with the expectation that sediment concentration decreases with distance from the immobile bed. We hypothesize that the bins with considerably increased magnitude of the return signal correspond to the layer of rolling and sliding bedload sediment, and that bins characterized by the base level of acoustic backscatter magnitude correspond to clear water flow. Bins in between the rolling and sliding bedload transport layer and the clear water flow layer are assumed to correspond to saltating bedload.

Second, the signature of the time-series of the I signal is investigated in bins near the bed. Figure 6 focuses on a 0.2 s time-series sampled at PRF = 1000 Hz in the bin containing the immobile bed and the three overlaying bins. According to the definition (Equation (2)), the I signal produced by a moving acoustic scattering source should fluctuate around a zero value. Figure 6 clearly shows an offset in the time-averaged value of the I signal, especially for bins 57 and 58. This offset is due to imprecision in the analog demodulation of the measured signal. In order to prevent biased estimates, it is important to remove this offset from the signal before estimating the Doppler frequency according to Equation (4). The increase in magnitude of the raw return signal towards the bed observed in Figure 2 can be recognized in the increasing amplitude of the I fluctuations towards the bed in Figure 6. The I signal in bin 55 shows oscillations with a frequency and amplitude that varies in time, as can be expected for flow velocities in clear water. According to Hurther and Thorne (2011) and Naqshband et al. (2014b), the zero velocity and highest sediment concentration at the immobile bed surface, estimated within bin 58, should in theory correspond to a constant *I* value of high amplitude with negligible variance. Figure 6 shows that the measured amplitude is not always constant, but that sequences of fluctuating voltage occur. These sequences represent the intermittent passage of bedload particles that roll and slide on the immobile bed (cf. section “ADVP configuration and data analysis procedures” and Figure 4).

[Figure 6]

Third, the power spectral densities of the *I* signals simultaneously recorded by the four receivers are investigated. According to the theory outlined in the introduction, the frequency of the fluctuating *I* signal is proportional to the velocity of the acoustic scatterers. Hence, the power spectral density of the *I* signal represents the turbulent fluctuations of the velocity of the acoustic scatterers (Traykovski 1998, his appendix A). Figure 7 shows these power spectral densities in the bins corresponding to the estimated layers of rolling and sliding bedload, saltating bedload, and clear water. For the bin in clear water, these spectral densities are near Gaussian, as expected for turbulent velocity fluctuations. The peak value corresponds to a velocity of about 0.4 m s^{-1}, which compares favourably with the time-averaged velocity estimated using the pulse-pair algorithm (Equation 4, Figure 3b). The lower and higher values represent the turbulent velocity fluctuations. Interestingly, however, the power spectral density is left-skewed in the bin that is assumed to correspond to the rolling and sliding bedload layer, which is more consistent with observations of bedload particle velocities (Drake et al. 1988; Rennie and Millar 2007; Lajeunesse et al. 2010; Furbish et al. 2012). In the assumed layer of saltating bedload, the spectral densities look like a combination of a Gaussian and a left-skewed profile.

[Figure 7]

Fourth, the signature of the time-series of the velocity is investigated in bins near the bed (Figure 8). Velocity fluctuations in the first two bins of the assumed clear water layer (bins 54 and 55) are similar and represent turbulent coherent structures. The velocity fluctuations in bin 56, corresponding to the assumed layer of saltating bedload, seem to be coherent with the fluctuations in the clear water layer, but the amplitude of the velocities is considerably reduced. The velocities in the assumed layer of rolling and sliding bedload (bin 57) show less coherence with the turbulent coherent structures in the clear water above. The velocity is considerably smaller in bin 58 containing the immobile bed surface. The non-zero velocities represent the intermittent passage of bedload particles that roll and slide on the immobile bed (cf. section “ADVP configuration and data analysis procedures” and Figure 4).

[Figure 8]

A similar analysis of the characteristics of the backscattered raw return signal *I* (Figures 2, 6, 7) and the time-series of the velocities (Figure 8) has been performed for all experiments. This analysis revealed a clear footprint of the bedload sediment transport in the raw return signals, which indicates that the moving bedload sediment grains are the main scattering sources. Because the ADVP measures the velocity of the scattering sources, this analysis provides a first indication that the velocities measured by the ADVP correspond to the velocities of the moving sediment particles. Moreover, this analysis corroborated the identification based on the profile of the time-averaged velocity (Figure 3b) of the bin containing the immobile-bed surface, the layer of rolling and sliding bedload, and the layer of saltating bedload.

Simultaneous ADVP measurements and videography

Figure 9 shows the results for the time-averaged velocities in the main series of experiments. All relevant information is provided in Table 2 for the experiments with low acoustic power and in Table S1 of the supporting information for the experiments with high acoustic power. The total duration of each experiment has first been divided into periods with quasi-constant conditions. The reference *z*-level has been taken as the lowest level of the immobile-bed surface during the total duration of each experiment. The rise of the immobile bed level during the passage of a dune in the Q630L experiment, for example, is visible in the shift to right of the measured velocity profiles in Figure 9a. Similarly, the important variations in the immobile bed level due the break up of the armour layer in the Q1000L experiment are clearly visible in Figure 9e.

[Figure 9]

For each of the periods with quasi-constant conditions, the vertical profile of streamwise velocity measured in water column bins within the sensitivity range of the ADVP (beyond gate 37) fit the log-law very well (Figure 9). However, measured velocities in the near-bed bins was systematically less than expected from the log-law.

In the near-bed zone, the bin containing the immobile-bed surface and the layers of rolling and sliding bedload, saltating bedload, and clear water have been identified from the time-averaged velocity profile and the profile of the magnitude of the backscattered raw return signal as described in the section “ADVP configuration and data analysis procedures”. The identification of these different layers was confirmed by the analysis of the backscattered raw return signal *I* and the time-series of the velocities as described in the section “Signature of the raw signals recorded by the ADVP”.

The gray shaded areas in Figure 9 represent the distribution functions of the sediment velocities based on the PTV treatment of the eleven sequences of videography in each experiment (e.g., periods marked by red lines in Figure 5). The average particle velocity computed from these distribution functions, also indicated in the figure, agrees well with the

ADVP estimation of the dominant bedload velocity, which occurs at the elevation where the slip velocity is maximum (cf. section “ADVP configuration and data analysis procedures”). The relative and absolute differences between the average particle velocity estimated from ADVP and videography in each experiments are 21 % ± 9% and 0.0275 m s^{-1} ± 0.0125 m s^{-1}, respectively. This absolute difference is much smaller than the velocity variation within one bin of the ADVP measurements (Figure 9).

The average bedload velocity in the Q795L experiment is similar to that in the Q630L experiment, which can be attributed to the armouring of the bed. The average bedload velocity in the Q1000L experiment is substantially higher. The highest velocities of bedload particles observed in the video images (highest velocities in the gray distribution functions) were only slightly smaller than the velocity measured with the ADVP at the top of the non-logarithmic flow layer near the bed (Figure 9). This observation supports the hypothesis that these fastest moving particles were saltating bedload particles that had less slip velocity than rolling and sliding bedload particles. The shape of the distribution functions based on the videography (Figure 9) resemble the shape of the power spectral density distributions of the velocities measured with the ADVP in the bedload layer (Figure 7), further suggesting that the latter represent the velocity of the bedload sediment particles.

For the three investigated conditions shown in Figure 9, each experiment with low acoustic power was immediately followed by an experiment with high acoustic power (Figure 2). The latter corresponds to the standard ADVP configuration for optimal flow measurements in the body of the water column, but may lead to magnitudes of the backscattered raw return signal *I* that are frequently out of the recording range of the receivers near the bed. The former corresponds to the ADVP configuration optimized for measurements near the bed. A better resolution of the sediment velocity would be expected with low acoustic power and a better resolution of the flow with high acoustic power.

Differences between results from experiments with low and high acoustic power were found to be insignificant and within the experimental uncertainty (Figure 9). However, for the Q795 experiments, only about 10 % of the raw *I(t)* signal had a magnitude outside the receivers' recording range in the bin containing the surface of the immobile bed in the experiment with low acoustic power (Figure 2; Figure 6d), whereas 36% was out-of-range in the experiment with high acoustic power (Figure 2). These results demonstrate the robustness of the pulse-pair algorithm (Equation 4), which provides accurate estimations of the average velocity even in the presence of a non-negligible number of out-of-range values of I and Q. An important conclusion from this result is that measurements of the bedload sediment velocities can be performed with the standard configuration of the ADVP.

[Figure 10]

Figure 10 shows time series of the velocities in the main series of experiments with low acoustic power. It compares the quasi-instantaneous velocities spatially averaged within the ADVP measurement volume estimated with the Optical Flow algorithm to those measured with the ADVP in the bin containing the surface of the immobile bed and the bin just above (Table 2), where the rolling and sliding bedload sediment transport occurs. As explained before, the upper part of the bin containing the surface of the immobile bed is situated in the flow where bedload sediment particles roll and slide on the immobile bed (Figure 4), whence the ADVP measures in that bin a non-zero velocity. As also explained before, both the ADVP measurement in the bin containing the surface of the immobile bed, and the Optical Flow algorithm provide an average sediment velocity that includes areas of zero velocity associated with immobile particles. This explains why they provide velocities that are substantially lower than those estimated with the PTV algorithm, which only considers moving sediment particles in the water column (Figure 9).

For the sake of clarity, only two 10 s sequences of videography are shown for each experiment. In the Q630L and Q795L experiments, both the magnitude and the time series of the quasi-instantaneous velocities estimated from the videography with the Optical Flow algorithm agree very well with those measured by the ADVP in the bin containing the immobile-bed surface (Figures 10a and 10b), indicating that most of the bedload sediment transport occurred in the form of rolling and sliding particles within the bin containing the immobile-bed surface. This complies with the observation that only partial transport of sediment occurred in these experiments (Table 1), and that the largest particles moving were smaller than the ADVP's bin size. In the Q1000L experiment, the temporal evolutions of the velocities estimated from the videography and measured with the ADVP are clearly related, but the velocities estimated with the Optical Flow algorithm are generally smaller than those measured with the ADVP. In this experiment, generalized intense sediment transport occurred (Table 1), and the largest particles moving were larger than the ADVP's bin size. The layer of rolling and sliding bedload particles was at least two bins thick, and overlaid by a layer of smaller and faster moving saltating bedload particles of at least three bins thick (Figures 9e and 9f) The underestimation of the bedload velocities in the Q1000L experiment by the Optical Flow algorithm is tentatively attributed to the fact that the algorithm only resolves the velocity of the largest and slowest bedload particles, whereas the ADVP resolves the velocity of all particles.

These results are further substantiated by the cross-correlations between the fluctuations of velocities measured with the ADVP in the bin containing the surface of the immobile bed and estimated with the Optical Flow algorithm. These cross-correlations are defined as:

$$C = \frac{\overline{u'_{ADVP} u'_{OF}}}{\sqrt{\overline{u'^{2}_{ADVP}}}\sqrt{\overline{u'^{2}_{OF}}}} \tag{6}$$

where the prime denotes the fluctuating component of the velocity time-series and the overbar denotes time-averaging. The cross-correlation for the Q1000L experiment are relatively low at C=0.22+/-0.04, which complies with the important deviations between the time-series measured by ADVP and Optical Flow (Figure 10c). The cross-correlations for the Q630L and Q795L experiments are considerably higher at C=0.41+/-0.04 and C=0.74+/-0.04, respectively. These values further indicate that the ADVP also resolves the details of the temporal fluctuations of bedload particle velocities.

Comparison to semi-theoretical formulae based on previous results

Figure 11 summarizes results from all experiments, including the second series of experiments with flow depths of 0.14 m and 0.24 m measured with the standard configuration of the ADVP with high acoustic power, and without simultaneous videography. All relevant information is provided in tabular form as supporting information. For each of these flow depths, ten different discharges were tested, ranging from conditions without sediment transport to conditions with generalized sediment transport. Figure 11 presents the bedload velocity and layer thicknesses measured with the ADVP as a function of the shear velocity u_*. In straight uniform open-channel flows, Nezu and Nakagawa (1993) have proposed a semi-theoretical logarithmic profile for the streamwise velocity, exponential profile for the turbulent kinetic energy, and linear profile for the streamwise-vertical turbulent shear stress, which all scale with the shear velocity. Fitting of the measured vertical profiles to these semi-theoretical similarity solutions provides three estimates of u_*. The average of these three estimates is used on the abscissa in Figure 11. Each of the experiments of the second series was also divided into periods of quasi-constant conditions. Because differences between different periods were relatively small, only one average result is reported in Figure 11 for each experiment.

[Figure 11]

Figure 11a reports the velocity of the bed load particles estimated from the ADVP measurements. For the main series of experiments, bedload velocity estimated from the videography with the PTV algorithm is also shown. For u_* smaller than 0.02 m s^{-1}, the bed is stable and no bedload sediment transport occurs. Note that $u_{*,cr}$ = 0.02 m s^{-1} corresponds to the critical shear velocity for the initiation of sediment transport for d_{50} based on the Shields criterion (Shields 1936). When bedload transport occurs, the bedload velocity increases with increasing shear velocity, in line with results reported in literature. According to Lajeunesse et al. (2010, their equations 26 and 27), the average velocity of bedload particles, $v_{bedload}$, can be written as:

$$v_{bedload} = a\left(u_* - u_{*,cr}\right) + 0.11 v_{settling} \tag{7}$$

where u_* and $u_{*,cr}$ are the shear velocity and the critical shear velocity for the initiation of bedload transport, respectively, and $v_{settling}$ is the characteristic settling velocity of the sediment. As mentioned above, the critical shear velocity for d_{50} is 0.02 m s^{-1}. According to Brown and Lawler (2003) the settling velocity for d_{50} is 0.118 m s^{-1}. Different values are reported in literature for the coefficient a. Based on experimental observations of sediment moving above a mobile bed, Lajeunesse et al. (2010) reported a value of 4.4 ± 0.2 whereas Fernandez-Luque and Van Beek (1976) reported a value of 13.2 ± 0.6. The latter value was also reported by Abbott and Francis (1977) and Lee and Hsu (1994) for a single grain particle entrained above a rigid rough bed. The a value proposed by Lajeunesse et al. (2010) was based on experiments with sediment diameters of d_{50} = 0.00115 m, 0.00224 m and 0.0055 m, and Shields parameters in the range from 0.006 to 0.24. Fernandez-Luque and Van Beek (1976) performed experiments with sediment diameters of d_m = 0.0009 m, 0.0018 m, and 0.0033 m, and ratios of the Shields parameter to the critical Shields parameter for the initiation of motion of 1.1 to 2.7. These experimental conditions are comparable to those in the experiments reported in the present paper. The bedload velocity according to equation 7 for both values of a = 4.4 and 13.2 envelops all data from the here reported experiments (Figure 11a).

Figure 11b reports the thickness of the layer of rolling and sliding bedload (defined in the section “ADVP configuration and data analysis procedures“ and indicated in Figure 9) estimated from the ADVP measurements, which increases as expected with increasing shear velocity. The resolution of the bedload layer thickness is obviously limited by the size of the ADVP measuring bins of 0.004 m. The estimated bedload layer thickness increases from about 1 bin (0.004 m) at low transport to about 2 bins at high transport (0.008 m). Based on the solution of the equations of motion for a solitary particle, van Rijn (1984, Equation 10) proposed the following equation for the bedload layer thickness:

$$thickness = 0.3\, d \left[d \frac{\left(\rho_s/\rho - 1\right) g}{\nu^2} \right]^{1/3} \left(u_*^2 / u_{*,cr}^2 - 1 \right)^{1/2} \qquad (8)$$

where d is a characteristic diameter of the bedload sediments, taken as d_{50} by van Rijn (1984), ρ_s and ρ are the densities of the sediment and the water, respectively, g is the gravitational acceleration and ν is the kinematic viscosity of the water. Van Rijn (1984) calibrated this equation based on experiments with a uniform sediment diameter of d = 0.0018 m and a shear velocity of 0.04 m s^{-1}. These parameters are in the same range as in the experiments reported herein. All data on the bedload layer thickness estimated from the ADVP measurements in the present experiments are constrained by two curves, corresponding to predictions based on Equation 8 for bedload sediment diameters of $d = d_{50}$ = 0.0008 m and d = 0.0015 m. Hence, the ADVP estimates of the bedload layer thickness comply with the equation and underlying experiments of van Rijn (1984).

It is noteworthy that results for the velocities and thicknesses are quite similar for experiments Q630 and Q795 in the main series of experiments, and strongly increase from

Q795 to Q1000. This behaviour can be attributed to the gradual formation of the armour layer in Q630, which limits bedload transport in Q795, and the break up of the armour layer in Q1000.

Comparison of standard ADVP configuration and ADVP configuration optimized for bedload measurements

Both for the sediment velocity in the bedload layer, and the thickness of the dominant bedload layer, results of the experiments with a flow depth of 0.24 m in the second series with standard ADVP configuration (Table S2 of the supporting information) agree well with results in the main series with ADVP configuration optimized for bedload measurements (Table 2). Experiments with similar hydraulic conditions are compared (Q630L vs. Q605H, Q795L vs. Q794H and Q795H, and Q1000L vs. Q897H). The relative and absolute differences between the average particle velocity estimated with standard and optimized ADVP configurations are 20 % ± 8% and 0.032 m s^{-1} ± 0.025 m s^{-1}, respectively. This absolute difference is much smaller than the velocity variation within one bin (Figure 9). Both ADVP configurations provided identical estimations of the thickness of the dominant bedload layer. This confirms that the standard ADVP configuration provides reliable estimations of the bedload characteristics. It is noteworthy that results for the velocities and thicknesses are quite similar for experiments Q630 and Q795 in the main series of experiments, and strongly increase from Q795 to Q1000. This behaviour can be attributed to the gradual formation of the armour layer in Q630, which limits bedload transport in Q795, and the break up of the armour layer in Q1000.

DISCUSSION AND CONCLUSIONS

Previous experiments have indicated that near-bed velocities can deviate from the logarithmic profile due to beam geometry effects, i.e. contamination of the near-bed bins by high intensity scatter from the immobile bed (Hay et al. 20121), and due to the presence of bedload sediment transport (Naqshband et al. 2014b). The ellipses of equal acoustic travel time for the near-bed bins have been drawn in Figures 1a and 1b for the ADVP configurations adopted in the here reported experiments. These purely geometrical considerations indicate a potential contamination zone due to beam geometry effects of approximately 0.01 m. This is a conservative estimation, however, which does not take into account that the acoustic power is maximal in the centre of the insonified beam and decays in a Gaussian way towards its edges. In all experiments without sediment transport reported in this paper, the ADVP resolved the law of the wall logarithmic velocity profile, including in the first bin above the immobile bed (Figure 3a). This indicates that the contamination zone due to beam geometry effects is smaller than 0.004 m. On the contrary, in all experiments with bedload sediment transport reported in this paper, velocities in the near-bed region where bedload sediment transport occurs were systematically smaller than expected from the logarithmic law of the wall (Figure 3a,b and Figure 9), similar to observations by Naqshband et al. (2014b). The deviating velocities occurred in a layer of approximately 0.004 m to 0.02 m from the immobile bed (Figure 3 and Figure 9). These observations indicate that the velocity deficit in the near-bed region is essentially related to the transport of bedload in the reported experiments.

Results from all three strategies corroborate the main hypothesis of the present paper that the ADVP does measure sediment velocities, also in the near-bed layer where bedload transport occurs. First, the backscattered raw return signals *I(t)* recorded by the ADVP’s receivers reveal a clear footprint of the bedload sediment particles. The magnitude of $I(t)$ in the bins where bedload sediment transport occurs clearly exceeds that of bins above in the clear water flow (Figures 2 and 6) , which is due to the fact that sediment particles backscatter considerably more acoustic energy than micro air-bubbles in the clear water

(Hurther et al. 2011). Thus, the sediment particles are the main scattering sources in the insonified water column, and it is therefore their velocity that is measured by the ADVP. Spectra of the $I(t)$ signals are near-Gaussian in the clear water and left-skewed near the bed where bedload sediment transport occurs. The latter distribution is characteristic for bedload sediment transport (Figure 7), in agreement with recent findings (Drake et al. 1988, Rennie and Millar 2007, Lajeunesse et al. 2010, Furbish et al. 2012). Second, results from the simultaneous videography of the bedload sediment transport are in good agreement with ADVP results. Time-averaged velocities measured with the ADVP in the layer of rolling and sliding bedload transport agree well with those estimated from the digital video images of the moving sediment with a particle tracking algorithm (Figure 9). Moreover, velocity time series (mean and fluctuating components) measured with the ADVP in the bin containing the immobile-bed surface agree well with the time series of the average bed velocity estimated with the Optical Flow algorithm (Figure 10). Third, ADVP based estimates of the bedload velocities and thickness of the bedload layer are in agreement with semi-theoretical formulae based on previous experiments proposed by Lajeunesse et al. (2010) and van Rijn (1984), respectively, for a broad range of hydraulic conditions (Figure 11).

The ADVP configuration optimized for bedload measurements only marginally performs better than the standard configuration for flow measurements, which also provides satisfactory estimates of the sediment velocity and transport layer thickness.

These findings corroborate the hypothesis of Hurther et al. (2011) and Naqshband et al. (2014b) that the ADVP can measure the time-averaged velocity of bedload particles, and the hypothesis of Naqshband et al. (2014a) that it also measures the temporal fluctuations of the particle velocities. The shear velocities in the reported experiments were comparable to those in the experiments of Naqshband et al. (2014a,b), but their sediment size was about 10 times smaller, leading to Shields numbers that were about 10 times higher, and resulting in more intense bedload transport and significant suspended load transport. Both the present study and Naqshband et al. (2014a,b) used a similar ADVP with carrier frequency f_0 =1 MHz, resulting in a wavelength of the emitted acoustic pulses of about $\lambda = c/f_0 = 0.0015$ m. The sediment particles were smaller than this wavelength in Naqshband's experiment, leading to Rayleigh backscattering of the acoustic pulse. The particles were larger than this wavelength in our experiments, leading to geometric scattering. These results indicate that the ADVP is able to measure turbulent bedload velocities and the bedload layer thickness for a broad range of sediment diameters and different regimes of scattering.

These results confirm that ACVPs (Hurther et al. 2011), which integrate an ADVP with an Acoustic Backscatter System (ABS), are able to measure turbulent sediment fluxes according to Equation (1). The ABS ability to measure sediment concentration in the entire water column, including the bedload layer, has been demonstrated (Naqshband et al. 2014b). When sediment transport occurs, the ADVP provides unbiased measurements of the sediment velocity u_s, even in the near-bed layer where bedload sediment transport occurs. Velocities of bedload sediment will be smaller than velocities of the surrounding water, whereas velocities of suspended load sediment will be about equal to velocities of the surrounding water. When no sediment transport occurs, the ADVP measures the velocity of the clear water flow. The presence or non-presence of sediment in the water column is indicated by the ABS measurements of concentration. The position of the surface of the immobile bed can independently be estimated from the ADVP measurements as in the present paper, and from the ABS measurements as done by Hurther et al. (2011).

The present paper has proposed straightforward criteria based on the shape of the velocity profile to identify the layers of rolling and sliding bedload, saltating bedload, and suspended load or clear water (Figures 3 and 9). As a complementary approach, Hurther et al. (2011) identified the suspended load layer based on characteristics of the concentration profile measured with ABS, and defined the bedload layer as the intermediate layer between the immobile bed and the suspended load layer. The identification of these different layers is mainly important for comparison to commonly used formulae for bedload and suspended load transport. It is of minor importance in practical applications, however, because the river morphology is mainly determined by the total sediment flux estimated according to Equation (1).

The reported ADVP bedload results are sensitive to vertical resolution of the ADVP system. The bin size in the reported experiments was 0.004 m, which is the minimum bin size of the applied ADVP. Uncertainty in the determination of the levels of the immobile-bed surface, the layer of rolling and sliding bedload, and the layer of saltating bedload is about half a bin. In this case, the uncertainty of about 0.002 m in the vertical elevation is comparable to the mean diameter of the sediment (d_m = 0.0023 m). Moreover, the near-bed velocities change considerably within one bin (cf. Figure 9). Using interpolated estimates of these levels corresponding to half a bin (included in tabular form in Table 2 for the main series of experiments with low acoustic power and in the supporting information for the other experiments) considerably reduces discrepancies between velocities measured with ADVP and estimated from the digital video images, as well as the scatter in Figure 11 (which is not based on half-bin interpolations). These observations highlight the importance of an optimal choice of the ADVP parameters, and especially the bin size, which should be small compared to the thickness of the bedload layer. Naqshband et al. (2014a) adopted a bin size of 0.003 m in their investigation of sediment fluxes over equilibrium dunes, which was the minimum bin size of their ADVP, whereas the broadband multifrequency ADVP developed by Hay et al. (2012 a,b,c) is capable of a bin size of 0.0009 m.

A major advantage of ADVP's is their versatility, and the possibility to optimize their configuration for particular applications. The bin size, for example, is constrained by the

$$V_{\max} = PRF \ \frac{c}{4 f_0}$$

wavelength of the emitted acoustic pulse, $\lambda = c/f_0$, and can be reduced by increasing the carrier frequency f_0, bearing in mind that the maximum unambiguously measureable velocity is inversely proportional to f_0 (Pinkel 1980).

(9)

PRF is also related to the maximum profiling range D_{max}, which represents the longest travel path of the acoustic pulse between emitter and receiver in the measured water column:

$$D_{\max} = \frac{c}{2PRF} \tag{10}$$

In the here applied ADVP configuration, D_{max} is slightly larger than twice the maximum height of the investigated water column. Combining the constraints in equations (9) and (10) leads to the well-known range-velocity ambiguity relations in pulse-coherent Doppler systems (Pinkel 1980):

$$4V_{\max}\frac{f_0}{c} < PRF < \frac{c}{D_{\max}} \quad \text{and} \quad V_{\max}D_{\max} = \frac{c^2}{4f_0} \tag{11}$$

These relations show that pulse coherent systems must trade off the bin size, maximum observable velocities and maximum range of profiling, depending on operating frequency. If operating frequency is increased to reduce bin size, then PRF could be increased to maintain the same maximum measurable velocity (Equation 9). However, the profiling range would be reduced (Equation 10). This is not a major drawback in sediment transport applications, where the main region of interest is located in the vicinity of the bed. The ADVP acoustic operating frequency can be optimized based on the transport velocity and thickness of the bedload layer as predicted, for example, by means of Equations (7) and (8). It is worth noting that these principles underlying the optimal choice of the operating frequency, PRF and profiling range of the ADVP configuration are identical in measurements of turbulent flow and measurements of sediment transport, although high sediment concentration may impede use of higher operating frequencies due to increased acoustic attenuation.

The ADVP and the data treatment procedure outlined in the present paper can be applied for sediment transport investigations in the laboratory and in the field. The standard set-up for field investigations would involve placing the ADVP transducers immersed in the flowing water about O(1m) above the surface of the immobile bed, in order to focus on the near-bed region where sediment transport occurs. The ADVP could be mounted on a standard platform as commonly used in field investigations in river and coastal applications. Such a set-up would also be appropriate to validate the in-field ADCP technique for measuring the apparent bedload velocity developed by Rennie et al. (2002), Rennie and Church (2010) and Williams et al. (2015).

The demonstrated capability of the ADCP (which integrate ADVP and ABS) to measure sediment fluxes, including bedload fluxes has important implications, because no reliable technique is at present available to measure sediment fluxes. The results broaden the application range of ADCP in laboratory and field investigations, and should lead to enhanced insight in the dynamics of sediment transport and morphodynamic processes. Follow-up studies are required in bespoke laboratory settings with an optimized simultaneous deployment of ADVP and high-speed videography, and possibly complementary physical sampling, in order to estimate the accuracy and uncertainty in the sediment velocity measurements, and to delimit the application range of the ADVP technique.

Acknowledgements

Blanckaert was partially funded by the Distinguished Visiting Scientist Program of the University of Ottawa, grant number 602311. Rennie was partially funded by a Visiting

Professor grant from École Polytechnique Fédérale de Lausanne and a Discovery Grant from the Natural Sciences and Engineering Research Council of Canada. We wish to thank uOttawa M.A.Sc. student Saber Ansari for performing the manual particle tracking used to validate the automated particle tracking algorithm. All data can be obtained from Koen Blanckaert (koen.blanckaert@epfl.ch).

REFERENCES

Abbott, J., and J. Francis (1977), Saltation and suspension trajectories of solid grains in a water stream, *Philos. Trans. R. Soc. London A*, 284, 225–254.

Ancey, C., and J. Heyman (2014), A microstructural approach to bed load transport: Mean behaviour and fluctuations of particle transport rates, *J. Fluid Mech.*, 744, 129-168.

Beutelspacher, A., and U. Rosenbaum (1998), *Projective Geometry: From Foundations to Applications*, Cambridge Univ. Press, Cambridge, UK, ISBN 0-521-48364-6.

Blanckaert, K. (2010), Topographic steering, flow recirculation, velocity redistribution, andbed topography in sharp meander bends, *Water Resour. Res.*, 46, W09506, doi:10.1029/2009WR008303.

Blanckaert, K., and H. J. de Vriend (2004), Secondary flow in sharp open channel bends, *J. Fluid Mech.*, 498, 353–380.

Blanckaert, K., and U. Lemmin (2006), Means of noise reduction in acoustic turbulence measurements, *J. Hydraulic Res.*, 44(1), 3-17.

Bose, S. K., and S. Dey (2013), Sediment entrainment probability and threshold of sediment suspension: exponential-based approach, *J. Hydr. Eng.*, 139(10), 1099-1106.

Bricault, M. (2006), Rétrodiffusion acoustique par une suspension en milieu turbulent: application à la mesure de concentration pour l’étude des processes hydrosédimentaires. PhD thesis, Grenoble Institut National Polytechnique.

Brown, P. P., and D. F. Lawler (2003), Sphere drag and settling velocity revisited. *J. Environmental Eng.*, 129(3), 222-231.

Cellino, M., and W. H. Graf (2000), Experiments on suspension flow in open channels with bedforms, *J. Hydraul. Res.*, 38, 289–298.

Church, M. (2006), Bed material transport and the morphology of alluvial river channels, Ann. Rev. *Earth and Planetary Sciences*, 34 , 325-354.

Crawford, A. M., and A. E. Hay (1993), Determining Suspended Sand Size and Concentration from Multifrequency Acoustic Backscatter, *J. Acoustical Soc. Am.*, 94(6), 3312-3324.

Drake, T. G., Shreve, R. L., Dietrich, W. E., Whiting, P. J., and L. B. Leopold (1988), Bedload transport of fine gravel observed by motion-picture photography, *J. Fluid Mech.*, 192, 193-217.

Ferguson, R. I., Ashmore, P. E., Ashworth, P. J., Paola, C., and K. L. Prestegaard (1992), Measurements in a braided river chute and lobe 1. flow pattern, sediment transport, and channel change, *Water Resour. Res.*, 28(7), 1877-1886.

Fernandez-Luque, R., and R. Van Beek (1976), Erosion and transport of bed-load sediment, *J. Hydraul. Res.*, 14, 127–144.

Frey, P., Ducottet, C., and J. Jay (2003), Fluctuations of bed load solid discharge and grain size distribution on steep slopes with image analysis, *Exp. Fluids*, 35 (6), 589{597.

Furbish, D. J, Roseberry, J. C., and M. W. Schmeeckle (2012), A probabilistic description of the bed load sediment flux: 3. The particle velocity distribution and the diffusive flux, *J. Geophys. Res.: Earth Surf*, 117(3), F03033.

Gaeuman, D., and R. B. Jacobson (2006), Acoustic bed velocity and bed load dynamics in a large sand bed river, *J. Geophys. Res.: Earth Surf.*, 111(2), F02005.

Guerrero, M., Rüther, N., Szupiany, R., Haun, S., Baranya, S., and F. Latosinski (2016), The Acoustic Properties of Suspended Sediment in Large Rivers: Consequences on ADCP Methods Applicability, *Water-MDPI*, 8(1), Article number 13.

Guerrero, M., Szupiany, R. N., and M. L. Amsler (2011), Comparison of acoustic backscattering techniques for suspended sediments investigations, *Flow Meas. Instrum.*, 22, 392-401.

Guerrero, M., Szupiany, R. N., and F. Latosinski (2013), Multi-frequency acoustics for suspended sediment studies: An application in the Parana River, *J. Hydraul. Res.*, 51, 696-707.

Hay, A. E., Zedel, L., Cheel, R., and J. Dillon (2012a), Observations of the vertical structure of turbulent oscillatory boundary layers above fixed roughness beds using a prototype wideband coherent Doppler profiler: 1. The oscillatory component of the flow, *J. Geophys. Res.:Oceans*, 117(3), C03005, doi:10.1029/2011JC007113.

Hay, A. E., Zedel, L., Cheel, R., and J. Dillon (2012b), Observations of the vertical structure of turbulent oscillatory boundary layers above fixed roughness using a prototype wideband coherent Doppler profiler: 2. Turbulence and stress, *J. Geophys. Res.: Oceans*, 117(3), C03006, doi:10.1029/2011JC007114.

Hay, A. E., Zedel, L., Cheel, R., and J. Dillon (2012c), On the vertical and temporal structure of flow and stress within the turbulent oscillatory boundary layer above evolving sand ripples, *Cont. Shelf Res.*, 46(1), 31-49.

Heitz, D., Héas, P., Mémin, E., and, J. Carlier (2008), Dynamic consistent correlation-variational approach for robust optical flow estimation, *Exp. Fluids*, 45(4), 595-608.

Heyman, J. (2014), A study of the spatio-temporal behaviour of bed load transport rate fluctuations. PhD thesis no 6256, EPFL, Lausanne, Switzerland.

Heyman, J., Mettra, F., Ma, H. B., and C. Ancey (2013), Statistics of bedload transport over steep slopes: Separation of time scales and collective motion, *Geophys. Res. Lett.*, 40 (1), 128-133.

Horn, B. K. P., and B. G. Schunck (1981), Determining optical flow. *Artificial Intelligence*, 17(1–3), August 1981 185-203, ISSN 0004-3702, http://dx.doi.org/10.1016/0004-3702(81)90024-2.

Hurther, D. (2001), 3-D acoustic Doppler velocimetry and turbulence in open-channel flow. PhD thesis no 2396, EPFL, Lausanne, Switzerland.

Hurther, D., and U. Lemmin (1998), A constant beamwidth transducer for three-dimensional Doppler profile measurements in open channel flow, *Meas. Sc. Techn.*, 9(10), 1706–1714.

Hurther, D., and U. Lemmin (2001), A correction method for turbulence measurements with a 3D acoustic Doppler velocity profiler, *J. Atm. Ocean. Techn.*, 18(3), 446-458.

Hurther, D., and U. Lemmin (2008), Improved turbulence profiling with field-adapted acoustic Doppler velocimeters using a bifrequency Doppler noise suppression method, *J. Atm. Ocean. Techn.*, 25(3), 452-463.

Hurther, D., and P. D. Thorne (2011), Suspension and near-bed load sediment transport processes above a migrating, sand-rippled bed under shoaling waves, *J. Geophys. Res.: Oceans*, 116(7), C07001.

Hurther, D., Thorne, P. D., Bricault, M., Lemmin, U., and J. M. Barnoud (2011), A multi-frequency Acoustic Concentration and Velocity Profiler (ACVP) for boundary layer measurements of fine-scale flow and sediment transport processes, *Coastal Engineering*, 58(7), 594-605.

Klar, M., Jehle, M., Jähne, B., Detert, M., Jirka, G. H., Köhler, H.-J., and T. Wenka (2004), Simultaneous 3-D PTV and micro-pressure sensor equipment for flow analysis in a subsurface gravel layer. *Proc. River Flow 2004*, 703-712. Eds. Greco, Carravetta, and Della Morte, Taylor & Francis Group, London.

Lajeunesse, E., Malverti, L., and F. Charru (2010), Bed load transport in turbulent flow at the grain scale: Experiments and modeling, *J. Geophys. Res.: Earth Surf.*, 115(4), F04001.

Latosinski, F., Szupiany, R. N., García, C. M., Guerrero, M., and M. L. Amsler (2014), Estimation of Concentration and Load of Suspended Sediment in a Large River by Means of Doppler Technology, *J. Hydraul. Eng*., 140(7), Article number 04014023.

Lee, H.-Y., and I.-S. Hsu (1994), Investigation of saltating particle motions. *J. Hydraul. Eng.*, 120(7), 831–845.

Leite Ribeiro, M., Blanckaert, K., Roy, A. G., and A. J. Schleiss (2012), Flow and sediment dynamics in channel confluences, *J. Geophys. Res.: Earth Surf.,* 117(1), F01035, doi:10.1029/2011JF002171.

Lemmin, U., and T. Rolland (1997), Acoustic velocity profiler for laboratory and field studies, *J. Hydr. Eng.*, 123(12), 1089–1098.

Lhermitte, R., and R. Serafin (1984), Pulse-to-pulse coherent Doppler sonar signal processing techniques, *J. Atm. Ocean. Tech.*, 1(4), 293-308.

Lucas, B. D., and T. Kanade (1981), An Iterative Image Registration Technique with an Application to Stereo Vision, *Proc. of 7th Int. Joint Conf. on Artificial Intelligence*, Vancouver, Canada, 674–679.

Martin, R. L., Jerolmack, D. J., and R. Schumer (2012), The physical basis for anomalous diffusion in bed load transport, *J. Geophys. Res.: Earth Surf.*, 117(1), F01018.

Mettra, F. (2014), Morphodynamic mechanisms in steep channels: from local processes to large-scale evolution. PhD thesis no 6065, EPFL, Lausanne, Switzerland.

Miller, K. S., and M. M. Rochwarger (1972), Covariance approach to spectral moment estimation, *IEEE Trans. Inform. Theory*, 18(5), 588-596.

Moore, S. A., Le Coz, J., Hurther, D., and A. Paquier (2013), Using multi-frequency acoustic attenuation to monitor grain size and concentration of suspended sediment in rivers, *J. Acoust. Soc. Am.*, 133(4), 1959-1970.

Mulhoffer L. (1933), Untersuchungen über der Schwebstoff und Geschiebeführung des Inn nächst Kirchbichl, Tirol [Investigations into suspended load and bedload of the River Inn, near Kirchbichl, Tirol], *Wasserwirtschaft*, Heft 1-6.

Muste, M., Yu, K., Fujita, I., and R. Ettema (2009), Two-phase flow insights into open-channel flows with suspended particles of different densities, *Env. Fluid Mech.*, 9(2), 161-186.

Naqshband, S., Ribberink, J. S., Hurther, D., Barraud P. A., and S. J. M. H. Hulscher (2014a), Experimental evidence for turbulent sediment flux constituting a large portion of the total sediment flux along migrating sand dunes, *Geophys. Res. Lett.*, 41(24), 8870-8878, doi:10.1002/2014GL062322.

Naqshband, S., Ribberink, J. S., Hurther, D., and S. J. M. H. Hulscher (2014b), Bed load and suspended load contributions to migrating sand dunes in equilibrium, *J. Geophys. Res.: Earth Surf.*, 119(5), 1043–1063, doi:10.1002/2013JF003043.

Nezu, I., and H. Nakagawa (1993), *Turbulence in Open Channel Flows*, 281 pp., A. A. Balkema, Rotterdam, Netherlands.

Nino, Y., and M. H. Garcia, M. H. (1996), Experiments on particle-turbulence interactions in the near-wall region of an open channel flow: Implications for sediment transport, *J. Fluid Mech.*, 326, 285-319.

Pinkel, R. (1980), Acoustic Doppler techniques, in *Air–Sea Interaction Instruments and Methods*, edited by F. Dobson et al., pp. 171–199, New York: Plenum Press.

Radice, A., Malavasi, S., and F. Ballio (2006), Solid transport measurements through image processing, *Exp. Fluids*, 41(5), 721-734.

Rennie, C. D., and M. Church (2010), Mapping spatial distributions and uncertainty of water and sediment flux in a large gravel bed river reach using an acoustic Doppler current profiler, *J. Geophys. Res.: Earth Surf.*, 115(3), F03035.

Rennie, C. D., and R. G. Millar (2007), Deconvolution technique to separate signal from noise in gravel bedload velocity data, *J. Hydraulic Eng.*, 133(8), 845-856.

Rennie, C. D., Millar, R. G., and M. A. Church (2002), Measurement of bed load velocity using an acoustic Doppler current profiler, *J. Hydraulic Eng.*, 128(5), 473-483.

Rennie, C. D., and P. V. Villard (2004), Site specificity of bed load measurement using an acoustic Doppler current profiler, *J. Geophys. Res.: Earth Surf.*, 109(F3), F03003.

Rolland, T., and U. Lemmin (1997), A Two-component Acoustic Velocity Profiler for Use in Turbulent Open-channel Flow, *J. Hydraul. Res.*, 35(4), 545–561.

Rogers, S. S., Waigh, T. A., Zhao, X., and J. R. Lu (2007), Precise particle tracking against a complicated background: polynomial fitting with Gaussian weight, *Phys. Biol.*, 4(3), 220-227.

Roseberry, J. C., Schmeeckle, M. W., and D. J. Furbish (2012), A probabilistic description of the bed load sediment flux: 2. Particle activity and motions, *J. Geophys. Res.: Earth Surf.*, 117(3), F03032.

Ruhnau, P., Kohlberger, T., Schnörr, C., and H. Nobach (2005), Variational optical flow estimation for particle image velocimetry, *Exp. Fluids*, 38(1), 21-32.

Seizilles, G., Lajeunesse, E., Devauchelle, O., and M. Bak (2014), Cross-stream diffusion in bedload transport, *Phys. Fluids*, 26(1), 013302.

Shen, C., and U. Lemmin (1999), Application of an acoustic particle flux profiler in particle-laden open-channel flow, *J. Hydraulic Res.*, 37(3), 407-419.

Shields, A. (1936), Anwendung der Aehnlichkeitsmechanik und der Turbulenzforschung auf die Geschiebebewegung [Application of similarity mechanics and turbulence research on shear flow]. Mitteilungen der Preußischen Versuchsanstalt für Wasserbau (in German) 26. Berlin: Preußische Versuchsanstalt für Wasserbau.

Singh, A., Fienberg, K., Jerolmack, D. J., Marr, J., and E. Foufoula-Georgiou (2009), Experimental evidence for statistical scaling and intermittency in sediment transport rates, *J. Geophys. Res.: Earth Surf.*, 114(1),F01025.

Smyth, C., Hay, A. E., and L. Zedel (2002), Coherent Doppler Profiler measurements of near-bed suspended sediment fluxes and the influence of bed forms, *J. Geophys. Res.: Oceans*, 107(C8), 19-1 - 19-20, doi: 10.1029/2000JC000760.

Spies, H., Beringer O., Gröning, H., and H. Haussecker (1999), Analyzing particle movements at soil interfaces, in *Handbook on Computer Vision and Applications*, edited by B. Jähne et al., vol 3, 699-718, Academic Press.

Stanton, T. P., and E. B. Thornton (1999), Sediment fluxes above a mobile sandy bed in the nearshore, *Coastal Sediments '99, Volume One, Proceedings of the 4th International Symposium on Coastal Engineering and Science of Coastal Sediment Processes*, 241-252.

Stanton, T. P. (2001), Bistatic Doppler velocity and sediment profiler device for measuring sediment concentration, estimates profile of mass flux from the product of mass concentration and three component velocity vector, Us Sec of Navy. Patent number US6262942-B1.

Thorne, P. D., and D. M. Hanes (2002), A review of acoustic measurement of small scale sediment processes, *Cont. Shelf Res.*, 22, 603-632.

Thorne, P. D., and P. J. Hardcastle (1997), Acoustic measurements of suspended sediments in turbulent currents and comparison with in-situ samples, *J. Acoust. Soc. Am.*, 101(5), 2603-2614.

Thorne, P. D., Hardcastle, P. J., and P. S. Bell (1998), Application of acoustics for measuring nearbed sediment processes: An integrated approach, *Oceans'98* - Conference Proceedings, Vols 1-3, 438-441.

Thorne, P. D., and D. Hurther (2014), An overview on the use of backscattered sound for measuring suspended particle size and concentration profiles in non-cohesive inorganic sediment transport studies, Cont. Shelf Res., 73, 97-118.

Thorne, P. D., Hurther, D., and B. D. Moate (2011), Acoustic inversions for measuring boundary layer suspended sediment processes, *J. Acoust. Soc. Am.*, 130(3), 1188-1200.

Traykovski, P. (1998), Observations and modeling of sand transport in a wave dominated environment, PhD thesis, Massachusetts Institute of Technology and Woods Hole Oceanographic Institution.

van Rijn, L. C. (1984), Sediment transport. Part I: bed load transport, *J. Hydraulic Eng.*, 110(10), 1431-1456.

Williams, R. D., Rennie, C. D., Brasington, J., Hicks, D. M., and D. Vericat (2015), Linking the spatial distribution of bed load transport to morphological change during high-flow events in a shallow braided river, *J. Geophys. Res.: Earth Surf.*, 120(3), 604-622.

Wilson, G. W. , and A. E. Hay (2015), Acoustic backscatter inversion for suspended sediment concentration and size: A new approach using statistical inverse theory, Continental Shelf Research, 106, 130-149.

Wilson, G. W. , and A. E. Hay (2015), Measuring two-phase particle flux with a multi-frequency acoustic Doppler profiler, Journal of the Acoustical Society of America, 138(6), 3811-3819.

Wright, S. A., Topping, D. T., and C. A. Williams (2010), Discriminating silt and clay from suspended sand in rivers using side-looking profilers. In Proceedings of the 2nd Joint Federal Interagency Sedimentation Conference, LasVegas, NV, USA, 27 June-1 July 2010.

Zedel, L., and A. E. Hay (2002), A three-component bistatic coherent Doppler velocity profiler: Error sensitivity and system accuracy, *IEEE J. Ocean. Eng.*, 27(3), 717-725.

Zedel, L., Hay, A. E., Cabrera, R., and A. Lohrmann (1996), Performance of a single-beam pulse-to-pulse coherent Doppler profiler, *IEEE J. Ocean. Eng.*, 21(3), 290-297.

Figure Captions

Figure 1: Acoustic Doppler Velocity Profiler (ADVP) and digital video camera. The ADVP consists of a central beam emitter surrounded by four receivers; only two receivers are shown in the Figure. The insonified water column is divided in bins. The fan-beam receivers are sensitive in a field with a wide opening angle, with maximum sensitivity along the receiver axis. The red arcs define the ellipses of equal acoustic path travel time between the send and receive transducers for the bed bin (bottom arc) and the first bin above the bed (top arc). (a) Standard ADVP configuration optimized for flow measurements in the body of the water column. The transducers are in a water-filled box that is separated from the flowing water by an acoustically transparent mylar film. The fan-beam receivers cover the entire water column, and the receiver axis is focused in the body of the water column. (b) ADVP configuration optimized for bedload measurements. The transducers are immersed in the flowing water. The fan-beam receivers only cover the lower half of the water column, and the receiver axis is focused on the bed level. (c) Simultaneous deployment of the ADVP optimized for bedload measurements and a digital video camera focused on the same near-bed sample volume.

Figure 2: Time-averaged magnitude of the backscattered raw return signal recorded by the receive transducers, I^2 [V^2], for the Q795L experiment with low acoustic power (blue, x) and the Q795H experiment with high acoustic power (red, o). The configuration with high acoustic power optimizes the signal-to-noise ratio in the water column but provides a magnitude of the backscattered signal that is frequently outside the recording range of the receivers in the bedload layer. The configuration with low acoustic power provides a backscattered signal that remains within the recording range of the receivers in the bedload layer. The vertical axis to the left is the bin number, which increases with distance from the ADVP. The vertical axis to the right is the distance above the surface of the immobile bed. The full black horizontal line indicates the assumed level of the surface of the immobile bed, the dashed brown horizontal line the top of the assumed layer of rolling and sliding bedload, and the dotted black horizontal line the top of the layer of saltating bedload. ADVP measurements in bin numbers smaller than 37 are outside the sensitivity range of the ADVP transducers for the present ADVP configuration.

Figure 3: Time-averaged ADVP profiles of the longitudinal velocity estimated with the pulse-pair algorithm (Equation 4). The dashed line represents a linear fitting of the measured velocity against log(30z/k_s). The distance (m) above the immobile bed is indicated by z, and the equivalent grain roughness k_s is taken as 0.01 m. In order to avoid singularities, the bin containing the surface of the immobile bed has been plotted at $z = 0.001$ m. (a) Experiments in the second series of test with nominal flow depth of 0.14 m (Table 1); (b) Experiment Q795L in the main series of experiment. The symbol (v) denotes experiments without bedload sediment transport, and the symbol (x) denotes experiments with bedload sediment transport.

Figure 4: Near-bed bins including the bin in which the surface of the immobile bed is situated. The upper part of that bin is situated in the flow where bedload sediment particles roll and slide on the bed. Therefore the bin containing the surface of the immobile bed is identified as the bin with minimum non-zero velocity measured by the ADVP. Figure on scale

Figure 5: Temporal evolution of the magnitude of the raw backscattered signal, I^2 [V^2], during the 614 s Q1000L experiment. The colorbar defines the scale of I^2. The vertical axis shows the part of the water column between bin numbers 50 and 65 where the magnitude reaches maximum values. The 614 s duration is divided in five periods of quasi-constant conditions. Digital videography was performed during sequences of 10 s with an interval of 60 s, as indicated by the labels V1 to V11.

Figure 6: In-phase component I [V] of the complex range gated backscattered raw return signal measured at PRF =1000 Hz by one of the receivers in the Q795L experiment from t = 2 s to 2.2 s after the beginning of the experiment.

Figure 7: Power spectral density of the four beam velocities in bins [3, 2, 1] above the bin that contains the surface of the immobile bed in the Q795L experiment. Velocity [m s^{-1}] on the abscissa is calculated from observed beam Doppler frequencies, and transformed to the horizontal component.

Figure 8: Time series of velocities sampled at a frequency of PRF/NPP = 31.25 Hz in the Q795L experiment in bins 54 and 55 (clear water), 56 (saltating bedload layer), 57 (rolling and sliding bedload layer), and 58 (containing the surface of the immobile-bed).

Figure 9: Results of time-averaged velocities measured with ADVP (profiles) and particle tracking videography (gray distribution functions) for experiments Q630 (top row), Q795 (middle row) and Q1000 (bottom row). Test with low (left column) and high (right column) acoustic power. Experiments have been divided into periods of quasi-homogeneous conditions (Table 1 and Table S1 in the supporting information; period 1: blue, period 2: green, period 3: black; period 4: cyan, period 5: mauve). Note that the horizontal axis only refers to the time-averaged velocities measured with ADVP, but has no relation to the distribution function based on the videography.

Figure 10: Time series of quasi-instantaneous velocities, including turbulent fluctuations, measured with ADVP in the bin containing the immobile bed and the bin just above (Figure 9 and Table 1) and estimated from the videography with the Optical Flow algorithm (thick red line) for experiments Q630L (top row), Q795L (middle row) and Q1000L (bottom row). The horizontal axis indicates time from the beginning of the experiment. Two 10 s sequences of videography are shown (Figure 5). Additional videos showing the bedload transport are provided online as supporting information.

Figure 11: a) Sediment velocity in the bed load layer as a function of the shear velocity u_*. measured with ADVP (black) and estimated from videos by PTV (grey). The two lines represent predictions according to Equation 7 for $a = 4.4$ and $a = 13.2$, respectively. b) Thickness of the layer of rolling and sliding bedload (indicated in Figure 9) estimated from

ADVP as a function of the shear velocity u_*. The two lines represent prediction according to Equation 8 for $d = d_{50} = 0.0008$ m and $d = 0.0015$ m. For both a) and b), circles represent the experiments with simultaneous videography (main series), squares the second series experiments with flow depth 0.14 m, and crosses the second series experiments with flow depth 0.24 m. Because results for different periods within the same experiment were not significantly different, only one data point per experiment is shown, obtained as the average of results of all periods.

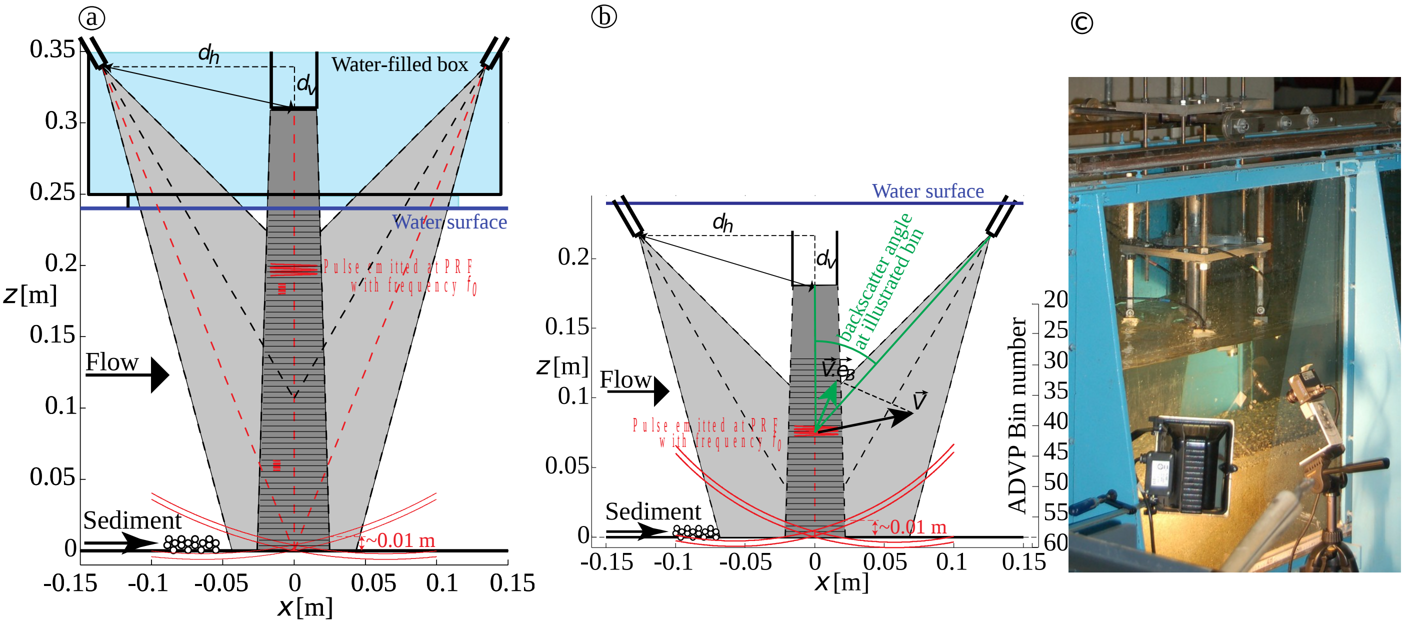

Figure 1: Acoustic Doppler Velocity Profiler (ADVP) and digital video camera. The ADVP consists of a central beam emitter surrounded by four receivers; only two receivers are shown in the Figure. The insonified water column is divided in bins. The fan-beam receivers are sensitive in a field with a wide opening angle, with maximum sensitivity along the receiver axis. The red arcs define the ellipses of equal acoustic path travel time between the send and receive transducers for the bed bin (bottom arc) and the first bin above the bed (top arc). (a) Standard ADVP configuration optimized for flow measurements in the body of the water column. The transducers are in a water-filled box that is separated from the flowing water by an acoustically transparent mylar film. The fan-beam receivers cover the entire water column, and the receiver axis is focused in the body of the water column. (b) ADVP configuration optimized for bedload measurements. The transducers are immersed in the flowing water. The fan-beam receivers only cover the lower half of the water column, and the receiver axis is focused on the bed level. (c) Simultaneous deployment of the ADVP optimized for bedload measurements and a digital video camera focused on the same near-bed sample volume.

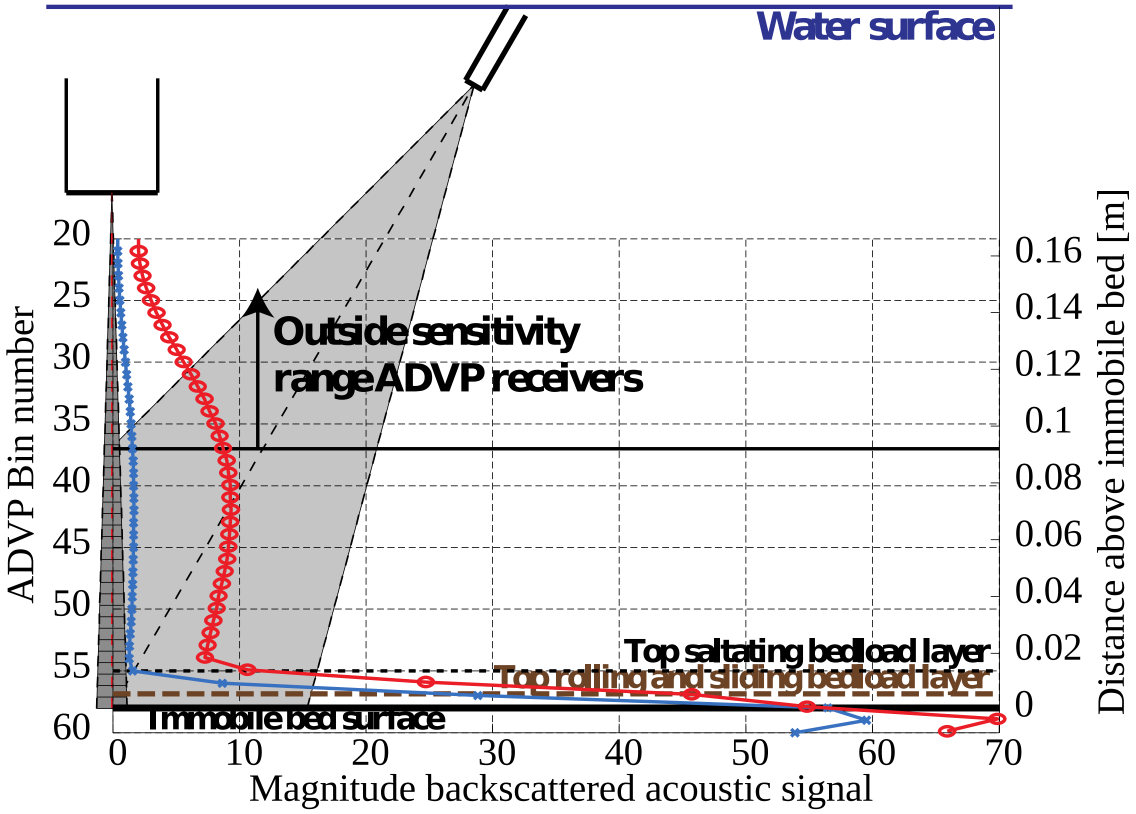

Figure 2: Time-averaged magnitude of the backscattered raw return signal recorded by the receive transducers, I^2 [V^2], for the Q795L experiment with low acoustic power (blue, x) and the Q795H experiment with high acoustic power (red, o). The configuration with high acoustic power optimizes the signal-to-noise ratio in the water column but provides a magnitude of the backscattered signal that is frequently outside the recording range of the receivers in the bedload layer. The configuration with low acoustic power provides a backscattered signal that remains within the recording range of the receivers in the bedload layer. The vertical axis to the left is the bin number, which increases with distance from the ADVP. The vertical axis to the right is the distance above the surface of the immobile bed. The full black horizontal line indicates the assumed level of the surface of the immobile bed, the dashed brown horizontal line the top of the assumed layer of rolling and sliding bedload, and the dotted black horizontal line the top of the layer of saltating bedload. ADVP measurements in bin numbers smaller than 37 are outside the sensitivity range of the ADVP transducers for the present ADVP configuration.

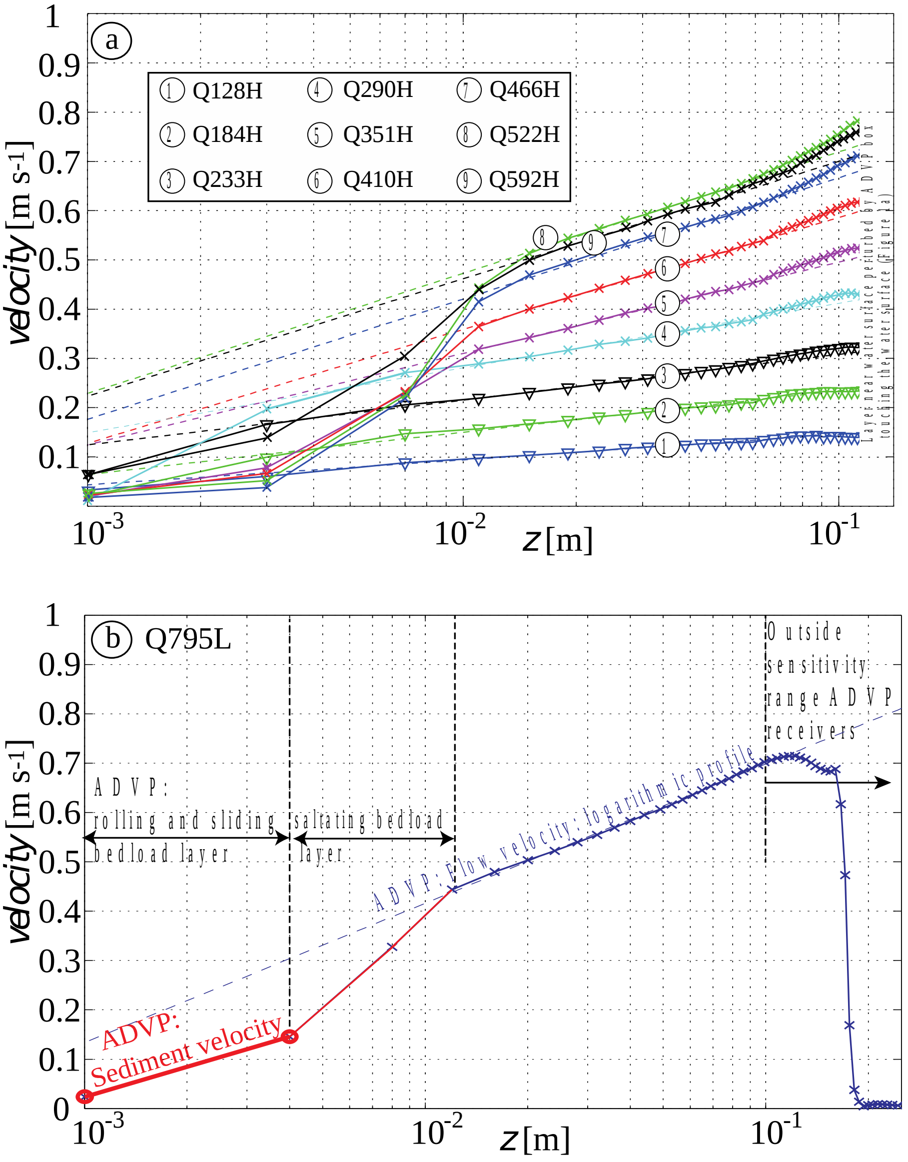

Figure 3: Time-averaged ADVP profiles of the longitudinal velocity estimated with the pulse-pair algorithm (Equation 4). The dashed line represents a linear fitting of the measured velocity against log($30z/k_s$). The distance in meter above the immobile bed is indicated by z, and the equivalent grain roughness k_s is taken as 0.01 m. In order to avoid singularities, the bin containing the surface of the immobile bed has been plotted at z = 0.001 m. (a) Experiments in the second series of test with nominal flow depth of 0.14 m (Table 1); (b) Experiment Q795L in the main series of experiment. The symbol (v) denotes experiments without bedload sediment transport, and the symbol (x) denotes experiments with bedload sediment transport.

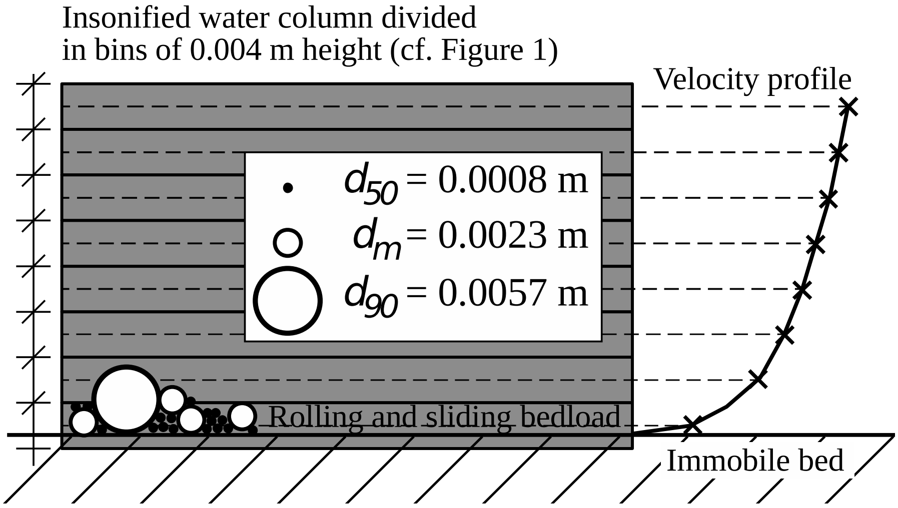

Figure 4: Near-bed bins including the bin in which the surface of the immobile bed is situated. The upper part of that bin is situated in the flow where bedload sediment particles roll and slide on the bed. Therefore the bin containing the surface of the immobile bed is identified as the bin with minimum non-zero velocity measured by the ADVP. Figure on scale

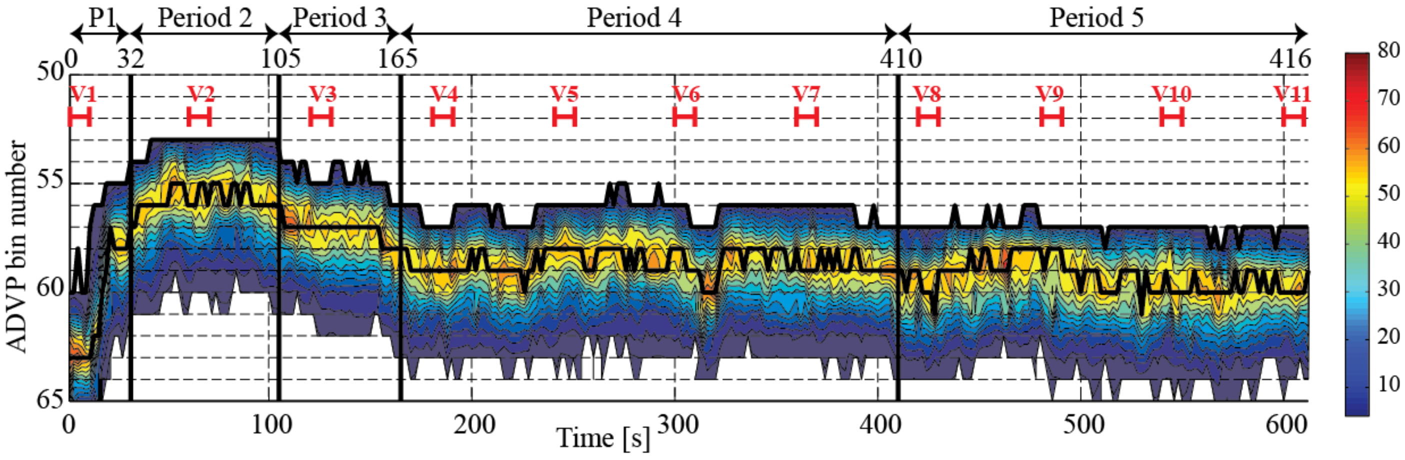

Figure 5: Temporal evolution of the magnitude of the raw backscattered signal, I^2 [V^2], during the 614 s Q1000L experiment. The colorbar defines the scale of I^2. The vertical axis shows the part of the water column between bin numbers 50 and 65 where the magnitude reaches maximum values. The 614 s duration is divided in five periods of quasi-constant conditions. Digital videography was performed during sequences of 10 s with an interval of 60 s, as indicated by the labels V1 to V11.

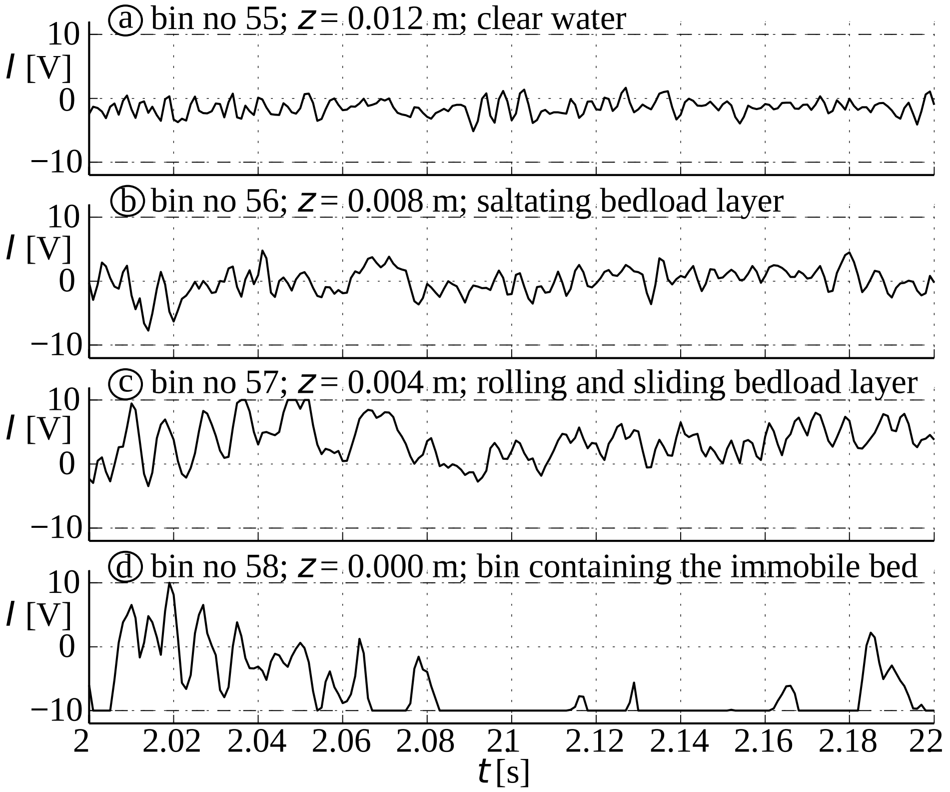

Figure 6: In-phase component *I* [V] of the complex range gated backscattered raw return signal measured at PRF =1000 Hz by one of the receivers in the Q795L experiment from t = 2 s to 2.2 s after the beginning of the experiment.

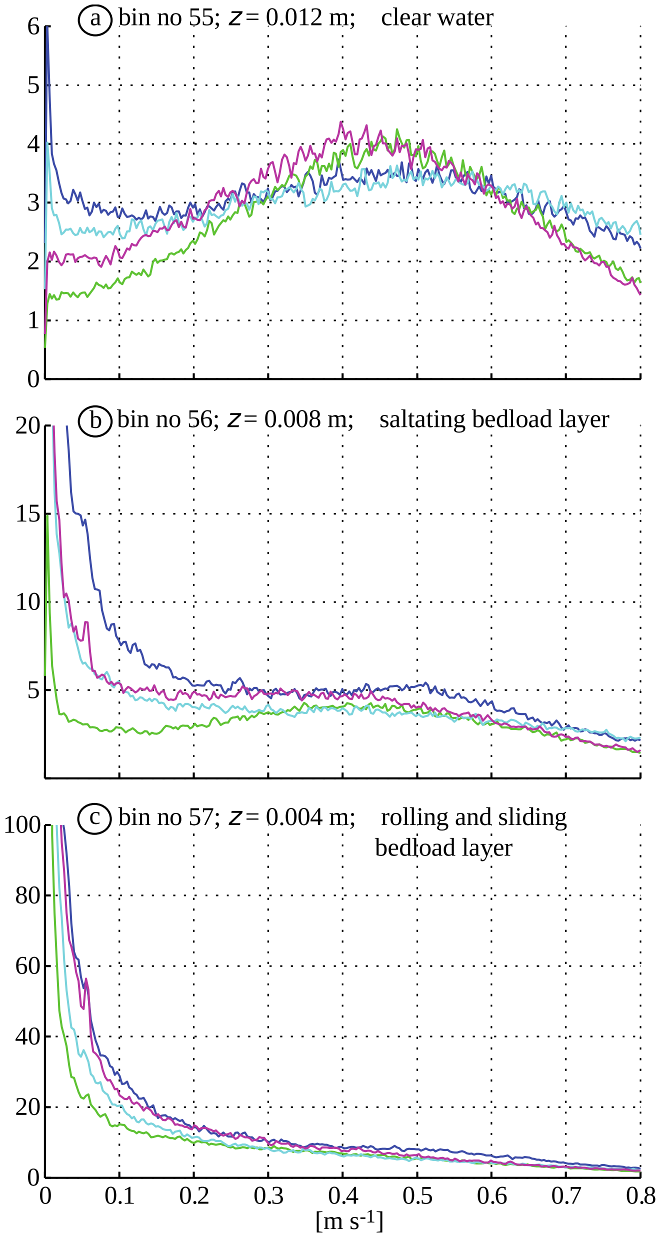

Figure 7: Power spectral density of the four beam velocities in bins [3, 2, 1] above the bin that contains the surface of the immobile bed in the Q795L experiment. Velocity [m s^{-1}] on the abscissa is calculated from observed beam Doppler frequencies, and transformed to the horizontal component.

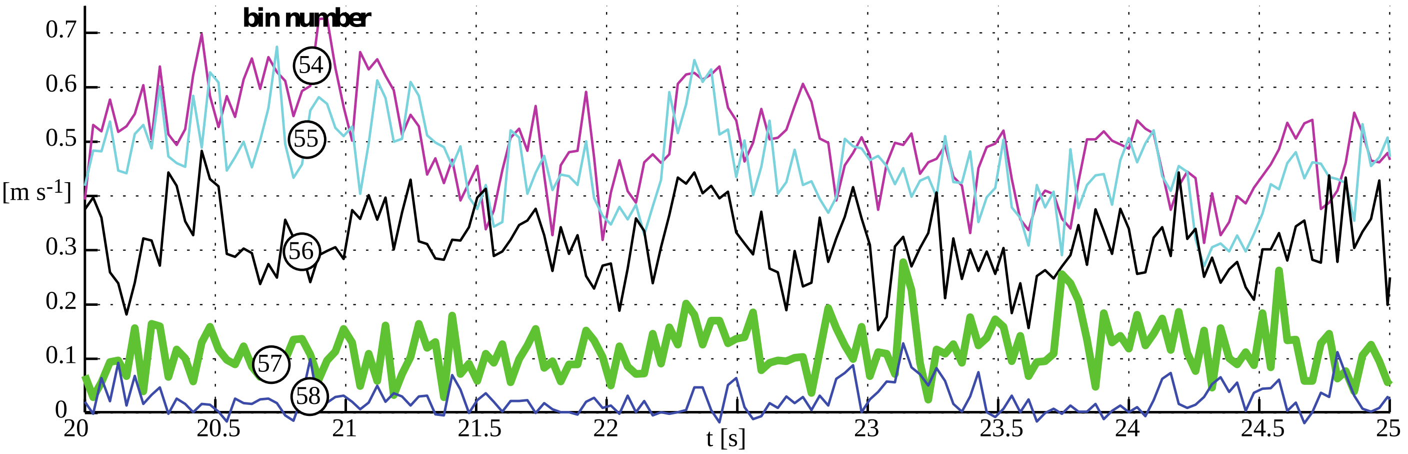

Figure 8: Time series of velocities sampled at a frequency of PRF/NPP = 31.25 Hz in the Q795L experiment in bins 54 and 55 (clear water), 56 (saltating bedload layer), 57 (rolling and sliding bedload layer), and 58 (containing the surface of the immobile-bed).

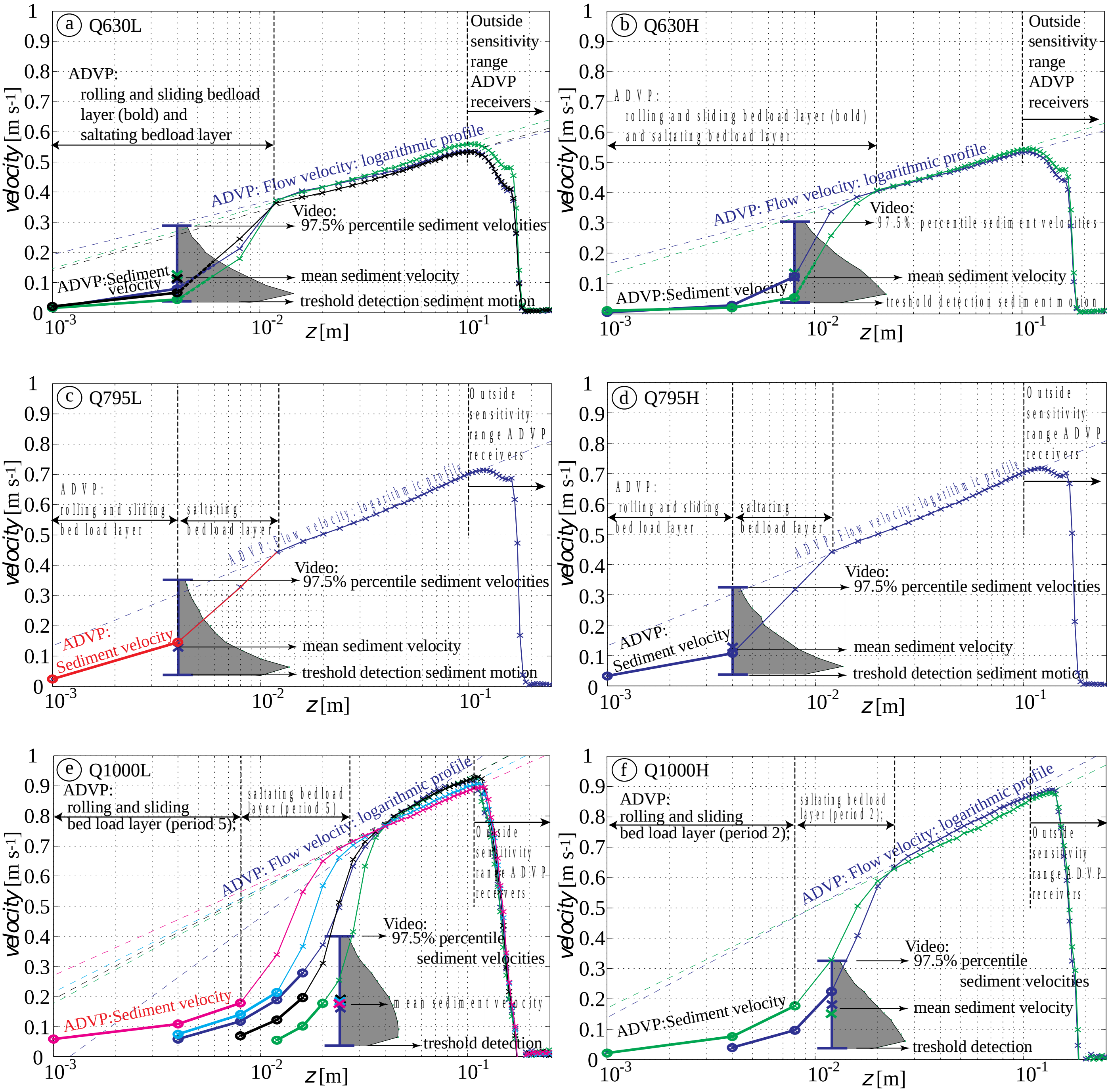

Figure 9: Results of time-averaged velocities measured with ADVP (profiles) and particle tracking videography (gray distribution functions) for experiments Q630 (top row), Q795 (middle row) and Q1000 (bottom row). Test with low (left column) and high (right column) acoustic power. Experiments have been divided into periods of quasi-homogeneous conditions (Table 1 and Table S1 in the supporting information; period 1: blue, period 2: green, period 3: black; period 4: cyan, period 5: mauve). Note that the horizontal axis only refers to the time-averaged velocities measured with ADVP, but has no relation to the distribution function based on the videography.

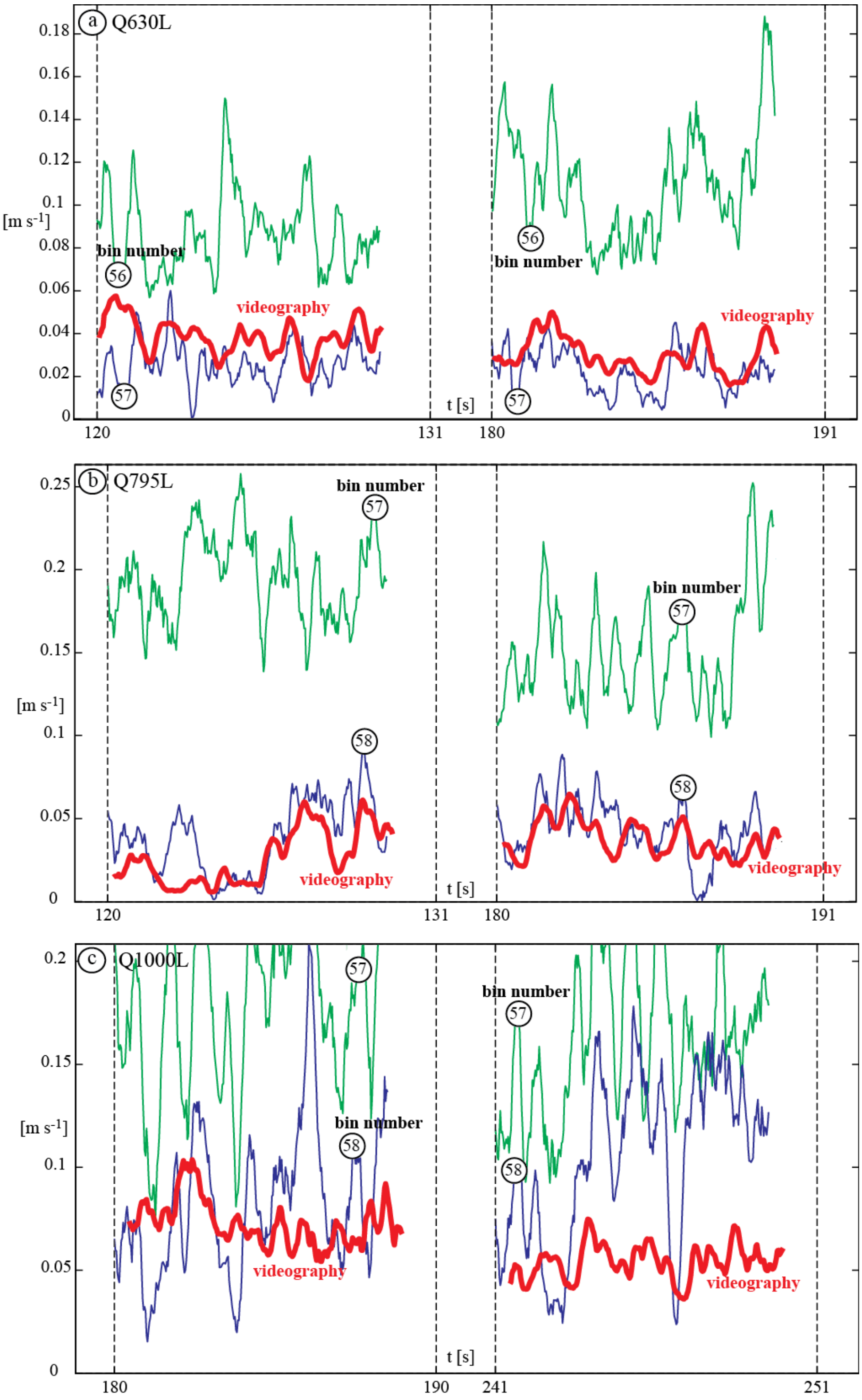

Figure 10: Time series of quasi-instantaneous velocities, including turbulent fluctuations, measured with ADVP in the bin containing the immobile bed and the bin just above (Figure 9 and Table 1) and estimated from the videography with the Optical Flow algorithm (thick red line) for experiments Q630L (top row), Q795L (middle row) and Q1000L (bottom row). The horizontal axis indicates time from the beginning of the experiment. Two 10 s sequences of videography are shown (Figure 5). Additional videos showing the bedload transport are provided online as supporting information.

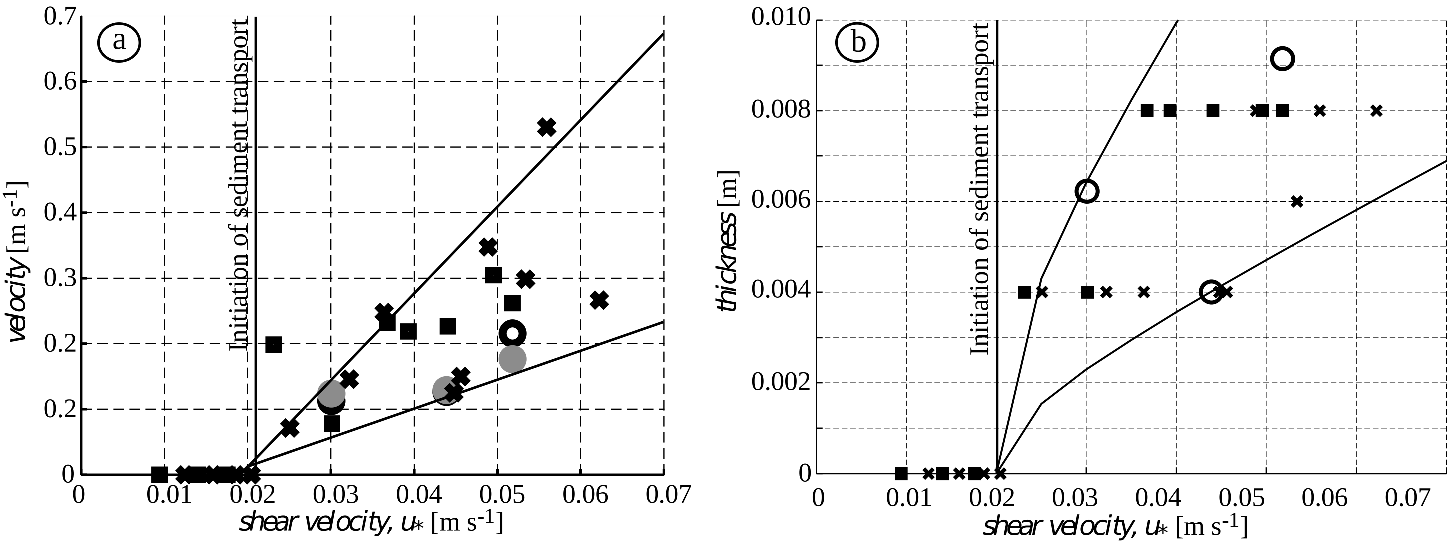

Figure 11: a) Sediment velocity in the bed load layer as a function of the shear velocity u_*. measured with ADVP (black) and estimated from videos by PTV (grey). The two lines represent predictions according to Equation 7 for a = 4.4 and a = 13.2, respectively. b) Thickness of the layer of rolling and sliding bedload (indicated in Figure 9) estimated from ADVP as a function of the shear velocity u_*. The two lines represent prediction according to Equation 8 for $d = d_{50}$ = 0.0008 m and d = 0.0015 m. For both a) and b), circles represent the experiments with simultaneous videography (main series), squares the second series experiments with flow depth 0.14 m, and crosses the second series experiments with flow depth 0.24 m. Because results for different periods within the same experiment were not significantly different, only one data point per experiment is shown, obtained as the average of results of all periods.